https://doi.org/10.5194/egusphere-2025-39
Preprint. Discussion started: 7 January 2025
© Author(s) 2025. CC BY 4.0 License.

Modelling the impact of anthropogenic aerosols on CCN concentrations over a rural boreal forest environment

Petri Clusius[1], Metin Baykara[2], Carlton Xavier[3,4], Putian Zhou[1], Juniper Tyree[1], Benjamin Foreback[1,6], Mikko Äijälä[6,1], Frans Graeffe[1], Tuukka Petäjä[1], Markku Kulmala[1], Pauli Paasonen[1], Paul I. Palmer[5], Michael Boy[1,6,7]

[1]Institute for Atmospheric and Earth Systems Research, University of Helsinki, P.O. Box 64, 00014 Helsinki, Finland
[2]Climate and Marine Sciences Department, Eurasia Institute of Earth Sciences, Istanbul Technical University, Maslak, Istanbul, 34469, Turkey
[3]Department of Physics, Lund University, SE-22100 Lund, Sweden
[4]Research Department, Swedish Meteorological and Hydrological Institute, SE-60176 Norrköping, Sweden
[5]School of GeoSciences, University of Edinburgh, Edinburgh, UK
[6]Atmospheric Modelling Centre – Lahti, Lahti University Campus, Lahti, Finland
[7]School of Energy Systems, Lappeenranta-Lahti University of Technology, Lappeenranta, 53850, Finland

Correspondence to: Petri Clusius (petri.clusius@helsinki.fi)

Abstract. The radiative properties of clouds depend partially on the cloud droplet number concentration, which is determined by the concentration of cloud condensation nuclei (CCN) when the clouds are formed. In turn, CCN concentrations are determined by the atmospheric particle size distribution and their chemical composition. We use a novel Lagrangian modelling framework to examine the origins and history of gas and aerosol components observed at the boreal forest measurement site SMEAR II, and their potential to act as CCN. This framework combines: a) global emission datasets, b) backward trajectories from the FLEXible PARTicle dispersion model (FLEXPART) airmass dispersion model, c) a detailed description of atmospheric chemistry and aerosol dynamics from the Model to Simulate the Concentration of Organic Vapours, Sulphuric Acid and Aerosol Particles (SOSAA). We apply this SOSAA-FP (FP standing for FLEXPART) framework to simulate a period from March to October 2018 with one hour time resolution, focusing on the concentrations of CCN between 0.1–1.2 % maximum supersaturation as calculated by the κ-Köhler theory (with respective dry particle diameter of activation ca. 175–35 nm). We find that the model PM_1 fraction of primary particles, sulfates and secondary organic aerosol correlate well with the observed organic aerosol and sulfate trends and explain most of the observed organic aerosol and sulfate PM_1 mass. Our results show that primary particle emissions play a considerable role in CCN concentrations even at a rural site such as SMEAR II. Changes in atmospheric cluster formation rates had a relatively weak impact on the CCN concentrations in the sensitivity runs. Enhanced cluster formation increased (decreased) the CCN concentrations for the highest (lowest) maximum supersaturation. Without any cluster formation our modelled median CCN concentrations changed by –48 % and +23 % for supersaturations of 1.2 % and 0.1 %, respectively, whereas omitting primary particle emissions had a decreasing effect in all calculated CCN supersaturation classes (–82 % and –33 % decrease in median CCN of 1.2 % and 0.1 % supersaturation, respectively). While the enhancing effect of cluster formation to high supersaturation (i.e., small diameter) CCN

https://doi.org/10.5194/egusphere-2025-39
Preprint. Discussion started: 7 January 2025
© Author(s) 2025. CC BY 4.0 License.

concentrations is unsurprising, the weak sensitivity to cluster formation rates and the decreasing effect to lowest supersaturation CCN was unexpected, as was the strong influence of anthropogenic primary emissions. The Lagrangian model framework showed its power, as it was possible to trace down the causes behind the unexpected outcomes by comparing how the particle population evolved along the trajectories in different sensitivity tests.

1 Introduction

The atmospheric energy budget is heavily influenced by water in all its phases. Undoubtedly the liquid and solid phases – found prominently in clouds – are far more complex when it comes to quantifying their influence on radiative forcing (RF). Clouds affect the path and intensity of downward and upward radiation in visible and thermal wavelengths by absorption and scattering. Broadly, the process of forming cloud droplets requires two ingredients: first, excess moisture – above 100 % relative humidity, i.e. supersaturation state – and second, the presence of cloud condensation nuclei (CCN), which act as condensation seeds for heterogeneous nucleation of water. The first condition is usually met where moist air is being lifted by convection, and the adiabatic cooling of the air brings the vapour below the dew point. Depending on the updraft velocity, which roughly determines the maximum achievable supersaturation, the critical diameter of the CCN (i.e. diameter above which over 50 % of particles activate), is commonly found between 40–100 nm (Dusek et al., 2006), or even below (Svensmark et al., 2024).

CCN can originate from primary particles that are directly emitted to the atmosphere (and possibly processed further in the atmosphere), or from new particle formation (NPF), where the particles are formed through clustering and condensational growth of atmospheric vapours. These two sources are separate only in the most ideal sense; in the atmosphere, particles are mixed due to coagulation, and secondary aerosol mass forms via gas-to-particle partitioning on both primary and NPF-particles. Consequently our definition that demarcates the two processes is not clearly defined, and remains difficult to determine with measurements alone (Kerminen et al., 2012). The origins of CCN are relevant to future climate predictions as it is likely that the anthropogenic emissions of primarily emitted particles and the precursor gases involved in NPF will change with emission mitigation policies, and will likely change further in the coming years due to the transition of fossil fuel based energy production and transport to renewables and nuclear energy.

NPF is estimated to contribute to a significant fraction of the global CCN. Paasonen et al. (2013) estimated that approximately half of the PN_{100nm} particles (corresponding approximately 0.2–0.3 % supersaturation) in continental Europe originate from direct primary emissions, that is, emissions of particles larger than 100 nm in diameter, while the rest is resulting from the growth of both NPF and emitted particles. Several model studies have shown that globally, about half of all CCN are secondary organic aerosol particles originating from NPF (Merikanto et al., 2009; Yu and Luo, 2009; Gordon et al., 2017), while other model studies suggest more modest effect. Pierce and Adams (2009) saw 12 % change in the average global boundary layer $CCN_{0.2\%}$ concentrations when nucleation rates were changed within 6 orders of magnitude, while Reddington et al. (2011) were able to reproduce boundary layer CCN_{50nm} to a good degree (R^2 0.8, NMB –18 %) without any nucleation

https://doi.org/10.5194/egusphere-2025-39
Preprint. Discussion started: 7 January 2025
© Author(s) 2025. CC BY 4.0 License.

on 15 European observation sites during the EUCAARI campaign in May 2008 using a global aerosol microphysics model. Gordon et al. (2017) estimated that NPF accounted for 54 % of the global CCN at 0.2 % supersaturation in the present-day environment. Pierce et al. (2014) reached a similar conclusion for particles between 50–100 nm diameter in a 1 year size distribution measurements at Egbert, Canada. Estimates vary still markedly depending on the location, anthropogenic influence and size class, and in general modelling the effect of NPF to CCN remains difficult (Ren et al., 2021).

Considerable work has been done to understand cluster formation in different conditions and geographical locations (e.g. Hirsikko et al., 2011; Kirkby et al., 2011; Almeida et al., 2013; Riccobono et al., 2014; Dunne et al., 2016; Chamba et al., 2023; Zhao et al., 2024). The starting point of NPF, formation of stable clusters, is known to occur through clustering of sulfuric acid and basic compounds such as ammonia or amines (Sipilä et al., 2010), but other pathways, involving for example large organic molecules or iodic acids are been observed in different environments and laboratory experiments (Elm et al., 2020, Zhao et al., 2024). Besides the rate of cluster formation, it is also important to consider their growth rates, as the clusters are quickly scavenged by larger particles. The growth of the sub-10 nm clusters is believed to come largely through condensation of (usually highly oxygenated) extremely low volatility organic vapours and sulfuric acid (Ehn et al., 2014). Consequently, it is important to understand the emission of VOCs and their subsequent oxidation and partitioning within the aerosol size distribution. Oxidation of the most abundant emitted biogenic volatile organic compounds (BVOC), isoprene, monoterpenes and sesquiterpenes, are known to produce a vast spectrum of low volatility vapours, many of which can condense on the smallest particle sizes, or even participate in cluster formation (Dada et al., 2023). Modelling particle growth via condensation of organic vapours is usually based on the saturation vapour pressure of the oxidation products, or parametrised in terms of mass yield, as is often done in global models. Regarding anthropogenic VOC emissions (AVOC), most models lack a mechanistic understanding of their autoxidation and the resulting components, contributing to the uncertainty in estimating human influence on secondary organic aerosol (SOA) formation and thereby CCN concentrations in urban areas. Steps towards closing this knowledge gap have been taken in the recent years (Garmash et al., 2020; Wang et al., 2021; Pichelstorfer et al., 2024). There is also evidence of heterogeneous chemistry between VOC oxidation products and aerosols, affecting SOA yields, but the global implications of these processes are still unclear.

Studies have linked BVOC emissions to CCN concentrations (e.g. Riipinen et al., 2011; Paasonen et al., 2013; Petäjä et al., 2021; Yli-Juuti et al., 2021), but due to the intertwined nature of primary and secondary aerosols, it is not clear how much of this link translates to the contribution of cluster formation specifically and NPF in general. Atmospheric chemical composition and aerosol processes in a particular location is generally affected by the airmass history, especially for components with long atmospheric lifetimes and processes with long timescales. While CCN concentrations are linked to high SOA mass and increased temperatures along trajectories, from local observations it is not clear what are the underlying independent processes during the upstream history of the airmasses. Assuming that local observations of aerosol processes are also taking place at a regional scale can lead to erroneous conclusions about the aerosol dynamics. For example, Hakala et al. (2023) showed that the apparent shrinkage of nucleation mode particles at Hada al Sham, Saudi-Arabia, was simply due to development of air mass transport in a manner that the particles arriving to the observation site during the afternoon/evening had

https://doi.org/10.5194/egusphere-2025-39
Preprint. Discussion started: 7 January 2025
© Author(s) 2025. CC BY 4.0 License.

grown less than those arriving before them, due to spatial and temporal heterogeneities in concentrations of vapours causing the growth. Studies at SMEAR II (Station for Measuring Ecosystem-Atmosphere Relations) station at Hyytiälä, Finland, have linked local NPF events to airmass trajectories arriving from the north-westerly or north-easterly direction over the North Atlantic or Arctic Ocean, consistent with conditions such as low condensation sink, ample short wave radiation and availability of sulfuric acid (Riuttanen et al., 2013; Vana et al., 2016; Dada et al., 2017). These conditions are somewhat different from those when high SOA loadings and increased temperatures along trajectory are observed. This implies that cluster formation and CCN formation are in general decoupled, and a favourable sequence of events is necessary for cluster formation to lead to CCN. Such would be the case of marine air arriving and advecting over forested area, eventually leading to increased CCN concentrations. However, the difficulty of separating primary particle emissions from secondary aerosol formation remains, as observation-based models aiming to describe measured aerosol types often struggle to classify aerosols as secondary or primary, and need very detailed chemical information to succeed (Zhang et al., 2009).

In this article, we utilize a one-dimensional aerosol and chemistry Lagrangian transport model to quantify the contributions of biogenic and anthropogenic secondary aerosol formation and primary anthropogenic emissions on the observed number concentrations and composition of CCN, and demonstrate how the seasonal variation of BVOC emissions and variability of the origins of the airmasses influences these contributions. We describe our recently developed modelling framework which can utilize detailed aerosol process models on the necessary spatial scale to describe the airmass history at least one week backwards. We have used it to address the following questions: 1) how much of the given CCN number concentration or composition at the SMEAR II station in rural Southern Finland can be attributed to primary or secondary sources? 2) how sensitive is the CCN number concentration to changes in emissions of some key ingredients and cluster formation rates? and 3) given possible future changes in the tested parameters, what can we expect to happen to CCN number concentrations? We concentrate here on three components that affect CCN concentration: cluster formation rates (NUC), anthropogenic primary number emissions (PNE) and BVOC emissions (BIO). For the benefit of the reader, Table 1 describes the abbreviations frequently used in this paper.

Table 1: Frequently used abbreviations

BIO	BVOC emissions in the model
NUC	Cluster formation rates in the model
PNE	Anthropogenic $PN_{1\mu m}$ particle number emissions in the model
f_I	factor of change in BIO, NUC or PNE
f_O	factor of change in some model output
$R = R(f_I, f_O)$	Model response to change in BIO, NUC or PNE, calculated from f_I and f_O
(A/B)VOC	(Anthropogenic/Biogenic) volatile organic compound
NPF	New particle formation, including formation of clusters and their growth
HOM	Highly oxygenated molecules, C:O ratio < 0.7 (Bianchi et al., 2019)

https://doi.org/10.5194/egusphere-2025-39
Preprint. Discussion started: 7 January 2025
© Author(s) 2025. CC BY 4.0 License.

CCN_X	Cloud condensation nuclei at supersaturation x %
[C]	brackets refer to concentration of *C* (cm^{-3} if not stated otherwise)
PSD	particle size distribution

2 Methods and data

The following sections describe the SOSAA-FLEXPART (later, SOSAA-FP) modelling framework, consisting of SOSAA (model to Simulate the concentrations of Organic vapours, Sulphuric Acid and Aerosols, (e.g. Zhou et al., 2017; Chen et al., 2021; Boy et al., 2022) and FLEXPART (FLEXible PARTicle dispersion model, Stohl et al., 1998; Stohl and Thomson, 1999; Stohl et al., 2005; Pisso et al., 2019) models, and its input data. In addition to a general overview, the individual steps necessary to use the SOSAA column model are described. We also include a description of the measurement data used to evaluate the model. For brevity, some details are left to the Supplementary material.

2.1 SOSAA-FLEXPART model framework (SOSAA-FP)

The SOSAA-FP framework simulates the effects of emissions, atmospheric chemistry, physics and meteorology on particle number size distribution, composition and gaseous compound concentrations during the long-distance transport to a chosen point location. SOSAA-FP uses global, gridded emission, concentration and meteorological data and is therefore not dependent on the availability of measurements at the location. However, as comparing a model to observations is beneficial in evaluating its performance, we chose SMEAR II as the end point of the trajectories.

SOSAA-FP consists of a 1-dimensional column model SOSAA, that simulates atmospheric chemistry and aerosol physics along a FLEXPART trajectory. Nominally, the model follows a mean airmass trajectory, which is calculated in advance using FLEXPART in backward mode. During the SOSAA simulation, the model is constrained by meteorological conditions (we used ERA5: Fifth generation of ECMWF atmospheric reanalyses of the global climate dataset, Hersbach et al. (2018); Hersbach et al. (2020)) at the mean location of the transported air parcels. The concentrations of all gas phase compounds are calculated by the SOSAA chemistry module based on the emissions (and meteorology) along the trajectory, except for [O_3] that was read in throughout the simulation from the CAMS global atmospheric composition dataset. In addition, [CO] and [SO_2] were initialized using CAMS data. Similarly, the aerosol size distribution, concentrations and composition are calculated by the aerosol module. The chemistry and aerosol modules are updated with the mean emissions at any given location. These means were calculated using FLEXPART's Source Receptor Relationship output as weighting factors, and are discussed in more detail in Sect. 2.1.2. The losses of the gases and particles are modelled with a simplified dry deposition to the ground and vegetation, further discussed in Sect. 2.1.3. The SOSAA-FP framework is schematically presented in Fig. 1. Each simulated trajectory contains the history of the airmass arriving at the station at a given time, shown in Fig. 1 with the

https://doi.org/10.5194/egusphere-2025-39
Preprint. Discussion started: 7 January 2025
© Author(s) 2025. CC BY 4.0 License.

red frames. When the procedure is repeated for a set of trajectories, a time series at the station is obtained, represented in the schematics by the bottom surface plot showing the time series of the vertical profile of HOM monomer concentrations.

The SOSAA-FP framework involves many pre- and post-processing steps before the SOSAA model can be run. We have made these processes easier with a suite of processing scripts, which streamlines the data processing on an HPC computer. Similarly to the ARCA-box (Atmospherically Relevant Chemistry and Aerosol model, Clusius et al., 2022), the SOSAA trajectory model has a graphical user interface, which can be used in setting up the model and data analysis. With this software suite the SOSAA-FP framework can be straightforwardly applied from scratch to model any location on the globe, without the need to acquire site-specific input data for the models.

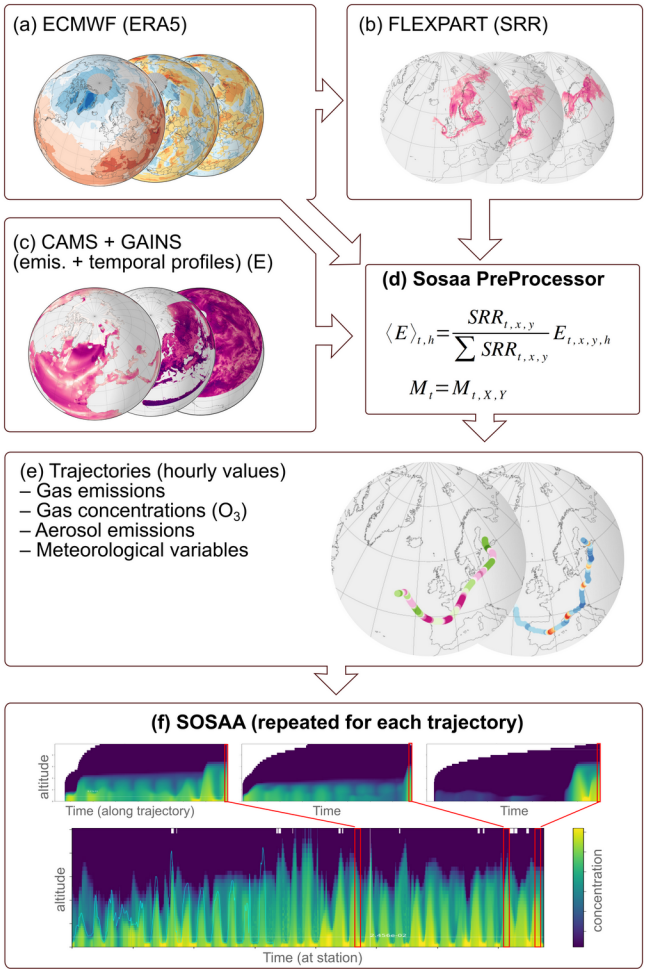

Figure 1: Schematic workflow of the SOSAA-FP framework. The boxes show the main steps taken to arrive at the results presented in this work, including (a) collection of reanalysis datasets from ERA5, (b) calculation of SRR (source-receptor relationship) with the airmass dispersion model FLEXPART, (c) collection of emission data from CAMS and GAINS, (d) processing data in a–c in to SOSAA input data, (e) collection of SOSAA input data, (f) chemical and aerosol transport simu-

https://doi.org/10.5194/egusphere-2025-39
Preprint. Discussion started: 7 January 2025
© Author(s) 2025. CC BY 4.0 License.

lation along trajectories with SOSAA. Bolded headlines show tools which are developed for this work. The arrows show the direction of the input data flow.

2.1.1 Flexpart trajectories

FLEXPART (FLEXible PARTicle dispersion model, Stohl et al., 1998; Stohl and Thomson, 1999; Stohl et al., 2005; Pisso et al., 2019) is a dispersion model used to trace airmasses both in the forward-time and backward-time mode (Seibert and Frank, 2004). In this study FLEXPART was used in the backward mode. FLEXPART needs gridded meteorological reanalysis data, and in this study, we used ERA5 dataset (Copernicus Climate Change Service, Hersbach et al., 2018), extracted in 0.5°×0.5° horizontal resolution and 137 (hybrid) vertical layers. FLEXPART starts with a predetermined number of particles (in this study inert and massless tracers), and disperses them forward or backward in time. This leads to a plume of tracers, generally spreading more the further away the air masses are from the release location. One of FLEXPART's outputs is the Source Receptor Relationship (SRR, in unit of seconds), which describes the time the air parcels are affected by emissions at different locations. When multiplied with the gridded emission fluxes, one gets the concentration at the receptor (the tracer release locations). Each output time (one hour interval) FLEXPART uses k-means clustering to group the dispersed particles into a few (in our case five) clusters, whose centre of mass locations are saved separately. From these clusters a single mean trajectory line is also calculated. In this study, some of the meteorological data (temperature, pressure, humidity, friction velocity and land-sea mask) was extracted from the single trajectory points from the ERA5 data, whereas the SRR-weighted means were used for all emissions, short wave radiation, leaf area index and albedo. The hourly mean mixing heights are calculated by FLEXPART using the lowest altitude where the Richardson number exceeds 0.25, and by taking a weighted mean of the tracer plume.

2.1.2 Emission Inputs

Since the SOSAA model is a 1-dimensional column model which is only run once per trajectory, the 3-dimensional emission and airmass dispersion fields need to be averaged to represent a mean trajectory. In order to calculate the mean emissions at any given time, normalized SRR were used as weighting factors in a pre-processing step (SOSAA PreProcessor, SPP, discussed in detail in the Supplementary material). In this study, the anthropogenic gas emissions come from Copernicus Atmosphere Monitoring Service (CAMS, Granier et al., 2019), specifically CAMS-GLOB-ANT dataset which is a globally gridded anthropogenic emissions inventory based on emissions provided by Emissions Database for Global Atmospheric Research (EDGAR) developed at Joint Research Center (JRC) (https://edgar.jrc.ec.europa.eu/, last access Jan 24, 2025, Crippa et al., 2018), and Community Emissions Data System (CEDS) (Hoesly et al., 2018). CAMS-GLOB-ANT dataset has a spatial resolution of 0.1°×0.1° in latitude and longitude and provides monthly averages of the global emissions of 36 compounds, 25 of which are speciated volatile organic compounds (Huang et al., 2017), including the main air pollutants such as NOx, NH_3, SO_2, CO and CH_4 for 16 emission sectors. These emission sectors are based on GFNR (Gridded Nomenclature For Reporting) sector classification. The methodology of how these emissions were generated for the 2000–2023 period is

https://doi.org/10.5194/egusphere-2025-39
Preprint. Discussion started: 7 January 2025
© Author(s) 2025. CC BY 4.0 License.

explained in detail by Soulie et al. (2023). To convert these emissions to hourly data CAMS-GLOB-TEMPO (Guevara et al., 2021) global emission temporal profiles are used. This temporal profile dataset has a spatial resolution of 0.1°×0.1° in latitude and longitude and includes monthly, weekly (day-of-the-week), daily (day-of-the-year) and diurnal temporal profiles for the main air pollutants (NOx, SO_2, NMVOC, NH_3, CO and $PM_{2.5}$, here used for number emissions of $PN_{1\mu m}$) and the greenhouse gases (CO_2 and CH_4). Temporal profiles are mainly for the following sectors; energy industry, refineries, residential combustion, manufacturing industry, road transport, aviation and agriculture.

For the biogenic gaseous emissions, CAMS-GLOB-BIO and CAMS-GLOB-OCE datasets were used. The emissions of BVOCs from vegetation were calculated with ERA5 meteorology and static land cover using the Model of Emissions of Gases and Aerosols from Nature (MEGAN v2.10, Guenther et al., 2012) on a 0.25°×0.25° grid as monthly mean values as well as monthly mean daily profiles (Sindelarova et al., 2022). These emissions include 25 BVOC species and chemical groups. Along with BVOCs from vegetation, SPP also process oceanic biogenic emissions using CAMS-GLOB-OCE dataset, and in this study emissions of dimethyl sulphide (DMS) with a grid resolution of 0.5°×0.5° and hourly temporal resolution were used.

Particle number emissions (PNE) and the respective particle size distributions (PSD) are obtained from Paasonen et al. (2016). This emission data set utilises the activity, technology, fuel and spatial gridding data from the GAINS model (Amann et al., 2011), more exactly for year 2020 within the ECLIPSE v5 CLE baseline scenario (Klimont et al., 2017). These data are combined with particle number emission factors developed by Paasonen et al. (2016), based on the European PNE inventory generated by Netherlands Organisation for Applied Scientific Research (van der Gon et al., 2009) during the EUCAARI project (Kulmala et al., 2011), but updated in terms of emission factors and size distributions for several source sectors, including road transport (based on TRANSPHORM database; Vouitsis et al., 2013) and residential combustion (based on wide literature review; Paasonen et al., 2016), and references therein), thus covering the dominant source sectors in European context. The diameter ranges of the size classes applied in the GAINS emissions are 3–10 nm, 10–20 nm, 20–30 nm, 30–50 nm, 50–70 nm, 70–100 nm, 100–200 nm, 200–400 nm, and 400–1000 nm. Since the GAINS size distribution is much coarser than that in SOSAA, using the emissions directly in SOSAA would have led to strong artefacts in the final modelled particle size distribution, and to overcome this, a smoothing function was applied to the calculated emissions that preserved the total PM_1, PN_1 and the bin number concentration as well as possible (PN_1 and PM_1 error in the smoothed emissions was typically less than 0.5 %). The number emissions of the coarse mode (starting from around 230 nm) were gradually reduced in the attempt to have a better closure between the emitted masses calculated from PN_1 and PM_1 from ECLIPSE V6b Baseline scenario (Klimont et al., 2017). The scaling is further discussed in the Supplementary material.

Even though CAMS and GAINS datasets were used in this study, SPP can be easily configured to use any type of emissions inventories. For our purposes, the chosen datasets were most suitable as they are readily available and consistent with our modelling domain and general spatio-temporal resolution. The methods used in SPP to calculate the mean emissions along the trajectory is discussed in more detail the Supplementary material.

https://doi.org/10.5194/egusphere-2025-39
Preprint. Discussion started: 7 January 2025
© Author(s) 2025. CC BY 4.0 License.

2.1.3 SOSAA trajectory model

The chemistry and aerosol model is based on the SOSAA (model to Simulate the concentrations of Organic vapours, Sulphuric Acid and Aerosols, e.g. Boy et al., 2022; Chen et al., 2021; Zhou et al., 2017) and ARCA-box (Atmospherically Relevant Chemistry and Aerosol model, Clusius et al., 2022) models. The model simulates the chemistry and aerosol processes in a column from the surface up to 2.5 km altitude, divided into 45 layers with increasing depth. SOSAA models the vertical turbulent diffusion with the simple Grisogono K(z) scheme, originally developed for the EMEP air pollution model (Jeričević et al., 2010). The necessary input for it, friction velocity (against which K is scaling linearly) and boundary layer height (BLH) are taken from ERA5 and FLEXPART output, respectively: friction velocity is calculated from northward and eastward surface stresses, whereas BLH is the average mixing height at the dispersed FLEXPART tracer plume. With BLH = 1500 m and friction velocity = 1 m^{-1} s^{-1} the scheme gives a maximum K_h of 74 m^{-2} s^{-1}, occurring at around 315 m, or 0.21×BLH, whereas a minimum was set with $k \geq 0.01$ m^2 s^{-1}, in practice applied above the boundary layer.

Trajectory SOSAA uses a simplified dry deposition scheme where the losses of the aerosols in the first 20 m were calculated using the low and high vegetation leaf area index from ERA5 as scaling factor. Particles were deposited with gravitational settling, impaction, interception and Brownian deposition by treating the canopy as needle-leaf tree everywhere. The evaluation with SOSAA dry deposition velocities against literature are in the Supplementary material.

Modelling dry deposition of gaseous compounds requires detailed information on the land use types and surfaces. To simplify the modelling setup the dry deposition was approximated with a single loss rate of 10^{-4} s^{-1} in the first 20 m (nominal canopy height) for all gaseous compounds.

Wet deposition, or cloud scavenging was not modelled in this study. As SO_2 has a large sink in the cloud droplets, and is subsequently removed with rain-out, omitting wet deposition would lead to overestimation of SO_2. At its current state SOSAA-FP does not model aqueous phase particle chemistry and the uptake of inorganic compounds, and to counterbalance this omission in SOSAA-FP, we applied a constant factor of 0.5 for all SO_2 emissions.

The chemistry scheme used in SOSAA for this study is based on a subset of the Master Chemical Mechanism (MCM 3.3.1 Jenkin et al., 1997; Saunders et al., 2003; Jenkin et al., 2015), and is augmented with the Peroxy Radical Autoxidation Mechanism (PRAM, Roldin et al., 2019), which simulates the autoxidation reactions of monoterpenes. The MCM subset was selected so that a reasonable mapping of the CAMS emissions to the chemistry system could be achieved. The selected precursors and their mappings are shown in Table S1.

SOSAA chemistry module solves the time-evolution of the 3542 chemical species and 11334 reactions in a 60 second time step, and is based on the Kinetic PreProcessor (https://kpp.readthedocs.io/en/latest, last access Jan 24, 2025, Lin et al., 2023). As the chemistry module is identical to that of the ARCA box, the interested reader is referred to Clusius et al. (2022), which describes the kinetic chemical system, solvers and calculation of photochemical reaction rates in detail.

The aerosol module follows that of ARCA box, which uses a sectional particle size distribution and simulates formation of stable atmospheric clusters via the ACDC module (Atmospheric Cluster Dynamics Code, Olenius et al., 2013), condensa-

https://doi.org/10.5194/egusphere-2025-39
Preprint. Discussion started: 7 January 2025
© Author(s) 2025. CC BY 4.0 License.

tional growth and Brownian coagulation as described in Clusius et al. (2022). In this study we used 60 logarithmically spaced particle size bins ranging from 1.07 nm to 2 µm in diameter and using the fully stationary method of distributing particles after growth and coagulation. The condensation of 600 lowest volatility organic compounds from the chemistry was simulated using the Analytical Prediction of Condensation scheme (APC, Jacobson, 1997; Jacobson, 2002). There are different parametrisations for estimating the volatilities and their temperature dependencies, and in this study, we used the volatility basis set (VBS) method as suggested in Stolzenburg et al. (2022) (Eqs. 10, 11 and 12). The necessary parameters for the reference saturation concentration at 300 K were those in Stolzenburg et al. (2018) for products originating from monoterpene peroxy radical autoxidation chemistry, and those in Donahue et al. (2011) for all other compounds. Condensation of sulfuric acid is calculated assuming a zero saturation vapour pressure. The SOSAA aerosol module does not calculate the ion balance and the uptake of water and soluble inorganics, but a rough estimation of the uptake of ammonia and nitric acid to particles was made in order to not underestimate the growth of nucleation and Aitken modes. The uptake of nitric acid was estimated by using the collision rate scaled with relative humidity so that the effective collision rate was

$$CR_{HNO3,eff} = MAX\left(0, \frac{RH-60}{40}\right) CR_{HNO3} \quad (1)$$

The uptake of ammonia was estimated by adding two NH_3 molecules for each condensed H_2SO_4 molecule and one for each HNO_3 molecule when the gaseous NH_3 concentrations allowed this. The size-resolved sea salt particle fluxes were calculated following Ovadnevaite et al. (2014), which is a parametrisation that takes into account the sea state with means of the Reynolds number. For this study the parametrisation was simplified so that the Reynolds number (Re) was replaced with wind at 10 m height (U10) by equating the reported mean fluxes as a function of Re and U10 and solving for Re. This simplification does not take into account that the salt particle fluxes are different when the wind is increasing and the sea state is still developing, and when the sea state is matured – whereas the Reynolds number captures this behaviour Ovadnevaite et al., 2014). The sea salt emissions were multiplied by the sea fraction of the land-sea mask. Over the Baltic Sea, which is brackish water and has smaller fetch than the oceans, the sea salt emissions were reduced to 5 % of the calculated fluxes.

New particles from the nucleation module, primary particle or sea salt emissions were added to their respective size bins and assigned a composition. As the exact composition of primary particles is unknown, they are assigned a tracer composition, which enabled us to track them and their emission day in the model through all the processes.

The formation of stable clusters through neutral and ion-mediated pathways was calculated by the ACDC module using the H_2SO_4–NH_3 chemistry (Besel et al., 2020), where the cluster stabilities are based on energies calculated with DLPNO-CCSD(T)/aug-cc-pVTZ//ωB97X-D/6-31++G** level of theory. This dataset can be considered as the best estimate of pure H_2SO_4–NH_3 clustering efficiency, but it could underestimate the clustering in atmospheric conditions where other components could be taking part in the cluster formation. Other datasets, notably those calculated with the B3LYP/CBSB7//RICC2/aug-cc-pV(T+d)Z have actually shown better agreement with laboratory experiments (Almeida et al., 2013; Kürten et al., 2016), but as the modelled [H_2SO_4] showed some overestimation, the more conservative DLPNO chemistry was used.

https://doi.org/10.5194/egusphere-2025-39
Preprint. Discussion started: 7 January 2025
© Author(s) 2025. CC BY 4.0 License.

2.2 Model setup and analysis

In this work, the FLEXPART trajectories were calculated (and the SOSAA model was run) seven days backward. The gas concentrations started from zero with the exception of SO_2, CO and O_3, which were initialized using CAMS reanalysis data. The particle size distribution is initialized with two modes (with count median diameters at 14 and 52 nm) $PN_{2\mu m}$ 1250 cm^{-3}, and therefore we considered the first three days to be spin-up time, and the results shown here are generally focused on the last 96 hours before the station. We simulated the base scenario, where the model input data was used in their nominal values (with the exceptions discussed earlier). We also tested, how sensitive the modelled CCN concentrations are to a relatively small perturbation in key input emissions and processes. The parameters that were perturbed with a constant factor were a) all biogenic emissions (CAMS-BIO), b) anthropogenic particle number emissions (PNE) and c) the nucleation rates calculated by ACDC. Additionally, we simulated two extreme cases where d) nucleation and e) primary particle emissions were turned off. Where the first three simulations can be thought of testing the model base state, the latter two shift the model substantially from the base state. These simulations did not represent realistic future scenarios, but estimate the effects of anthropogenic particle emissions and atmospheric clustering on CCN concentrations separately, and, when compared with BASE, their effect to each other. The scenarios are summarized in Table 2.

Table 2: Description and names of the SOSAA simulations used in this study.

Scenario name	Description	Motivation
BASE	Nominal emissions, except SO_2 × 0.5	Reference case
SensiNUC	BASE, but formation rates × 3.0	Test CCN response to atmospheric cluster formation rates
SensiPNE	BASE, but anthropogenic particle emissions × 1.20	Test CCN response to anthropogenic particle emissions
SensiBIO	BASE, but all emissions from CAMS BIO × 2.0	Test CCN response to biogenic emissions
ZeroNUC	BASE, but formation rates → 0	Contribution of atmospheric clustering and primary anthropogenic emissions to CCN
ZeroPNE	BASE, but anthropogenic particle emissions → 0	

2.2.1 Calculation of modelled CCN concentration

The modelled CCN concentrations presented here are calculated for maximum supersaturations between 0.1 % and 1.2 %, using the κ-Köhler theory (Petters and Kreidenweis, 2007), which relates the water vapour saturation to particle dry and wet diameters taking into account their hygroscopicity, expressed with the κ-coefficient. For a given dry particle diameter and κ, the critical wet diameter and the corresponding saturation ratio S can be determined from the (local) maximum of κ-Köhler equation:

$$S(D_{p,w}) = \left(1 + \frac{\kappa_{D_{p,d}} D_{p,d}^3}{D_{p,w}^3 - D_{p,d}^3}\right)^{-1} \exp\left(\frac{4\sigma v_w}{R_g T D_{p,w}}\right) \quad (2)$$

where $D_{p,d}$ and $D_{p,w}$ are the dry and wet diameter of the particle, σ is the solute surface tension (here value of pure water was used), R_g is the ideal gas constant and T is the droplet temperature (we used the model temperature at ground level to compare with measured CCN).

https://doi.org/10.5194/egusphere-2025-39
Preprint. Discussion started: 7 January 2025
© Author(s) 2025. CC BY 4.0 License.

The particle hygroscopicity κ depends on the composition, and here we used bulk values for the main aerosol components. This simplification can be justified by the unknown activity coefficients of 600 condensing organic compounds, the resulting composition mixture and the generally unknown composition of the anthropogenic particle emissions. To get an idea of the range of uncertainty in the CCN concentration related to the hygroscopicity, a combination of lower and upper κ ranges were used (the chosen κ and the ranges are shown in Table S2).

The κ values for any given particle size in bin i was calculated using $\kappa_i = \sum_{j=1}^{N_{comp}} \kappa_j \nu_{j,i}$, where $\nu_{j,i}$ are the volume fractions of the components in bin i. Using these κ in Eq. (2), the critical maximum supersaturation as a function of particle size and κ for the model particle size distribution can be calculated. Finally, the CCN_S number concentration for a given supersaturation S (expressed in %) is the sum of particles whose $S_{crit} \leq S$.

2.2.2 Calculation of model response

This study focuses on creating a model which is able to simulate the CCN concentrations, and investigating how the CCN may be formed. As the framework consists of many steps and input data which include averaging over large areas and times, it is expected that the model will miss any variability that is smaller than the resolution of the input data. Any particular year and location has special conditions, which are not perfectly captured by the often very generic emission profiles in the data-sets. Even with these shortcomings, given the model is in a reasonable proximity with observations, we can test how the modelled CCN responds to different processes and input parameters. A perturbation test provides an estimate of the significance of a single input in a multivariate model. Furthermore, as it turns out, the extrapolations made with the responses are passable estimates of the effects of larger perturbations. For example, everything else being equal, if biogenic emissions increase by a factor of 2, with what factor does the CCN change?

We define the response R as a linear sensitivity to the input. We can write the response R in terms of two model run output Q_{BASE} and Q_{PERT}, and their respective inputs I_{BASE} and I_{PERT}, obtained from perturbed (PERT) and unperturbed (BASE) model runs, respectively

$$R = \frac{\frac{Q_{PERT} - Q_{BASE}}{Q_{BASE}}}{\frac{I_{PERT} - I_{BASE}}{I_{BASE}}} \quad (3)$$

which simplifies to

$$R = \frac{f_Q - 1}{f_I - 1} \quad (4)$$

where f_Q and f_I are the fractions Q_{PERT}/Q_{BASE} and I_{PERT}/I_{BASE}, respectively. In some sense the response describes the model's current state with respect to I, including its history, all other input, concentrations, weather conditions, geographic location and the emissions that follow from it. Like the model state, R varies in time and place, and due to the non-linear nature of the model, we assume that it is reasonable to use the linear sensitivity when f_I and f_Q are in proximity of 1 (however, if $f_I = 1$, R is not defined); in other words, we assume this state holds if the model is not perturbed too much. Note that the response is not

https://doi.org/10.5194/egusphere-2025-39
Preprint. Discussion started: 7 January 2025
© Author(s) 2025. CC BY 4.0 License.

necessarily bound between -1 and 1. In the results sensitivity is expressed in percent ($R_{\%} = R \times 100$ %). In addition to the linear response, we also tested a power function, where $R_{POW} = \ln(f_Q)/\ln(f_I)$. This function was better suited to predict the effect of the cluster formation rates in the ZeroNUC case (Table 2), and is further discussed in the Supplementary material.

2.2.3 Statistical descriptors used for model evaluation

We use normalized mean bias factor (B_{NMBF}, Eq. S3, Yu et al., 2006) and squared Pearson correlation coefficient (r^2) to evaluate model performance. In addition, mean fractional bias (MFB, Eq. S4) and mean fractional error (MFE, Eq. S5) were calculated for Fig. S2 as recommended by EPA (2007). To test if two distributions have unequal means or medians, we use Welch's t-test and Mood's median test, respectively. Of these, B_{NMBF} is the most useful, as it is statistically robust, symmetric around zero (B_{NMBF} = 0: no bias) and readily interpretable: the factor of under- or over-estimation is $f = (1+|B_{NMBF}|)^{sgn(B_{NMBF})}$ e.g. B_{NMBF}= –0.5 means the model has a negative bias by a factor of $(1+0.5)^{-1}$ = 1÷1.5, whereas B_{NMBF}= 0.5 means bias (by overestimating) by a factor of 1.5.

2.3 Measurement data for model evaluation

We used data from the SMEAR II (Station for Measuring Ecosystem–Atmosphere Relations; Haataja and Vesala, 1997; Hari and Kulmala, 2005) measurement station, (https://smear.avaa.csc.fi/, last access: Jan 24, 2025, Junninen et al., 2009) to evaluate the model results at the end of the trajectories. The SMEAR II station features continuous atmospheric measurements for a boreal forest stand since 1995 (Ilvesniemi et al., 2009; Keronen, 2017; Kolari et al., 2022), and houses a broad range of basic aerosol, trace gas, meteorological, ecological and soil measurement instruments on permanent basis and intensive measurement campaigns (e.g. Kulmala et al., 2009; Kulmala et al., 2011; Williams et al., 2011; Petäjä et al., 2016). The station represents boreal zone atmospheric "background" observations, with pronounced local and regional influence from forested areas (Williams et al., 2011), with very few local anthropogenic emission sources but some regional ones (Keronen, 2017). However, long-range transported air masses from continental Europe, British Isles, Eastern Europe, Southwest Russia (including St. Petersburg area), Kola Peninsula and Baltic regions regularly affect the aerosol, VOC and trace gas observations on site (Kulmala et al., 2000; Riuttanen et al., 2013; Patokoski et al., 2015; Keronen, 2017).

The modelling period was selected to be March to October 2018. The choice of the time was largely based on good data availability both for model input and model evaluation, but at the same time there were interesting meteorological features especially with regards to temperature. Compared to 30-year mean, March 2018 was colder and April slightly warmer, while during summer Finland experienced heat waves with lower than average precipitation in May and July, June temperatures being comparable to 30-year mean. Autumn was warmer than on average.

For this study a subset of comparable observation data was selected as follows. Atmospheric inorganic trace gas measurements from gas analysers (CO, O_3, NO_X, SO_2, Keronen, 2017), the volatile organic compounds (VOC) concentrations continuously measured with a proton transfer reaction mass spectrometer (PTR-MS, Lindinger and Jordan, 1998; Taipale et al.,

https://doi.org/10.5194/egusphere-2025-39
Preprint. Discussion started: 7 January 2025
© Author(s) 2025. CC BY 4.0 License.

2008; Blake et al., 2009). Aerosol particle number size distributions between 3–1000 nm in diameter, observed with with a differential mobility particle sizer (DMPS, Aalto et al., 2001) and CCN concentrations with cloud condensation nuclei counter (CCNC, Roberts and Nenes, 2005; Paramonov et al., 2015). Aerosol particle chemical composition was obtained from using the Aerosol Chemical Speciation Monitor (ACSM, Ng et al., 2011; Heikkinen et al., 2020), which offers a standard speciation into organics, sulfates, nitrates, ammonia and chlorides. When the measurement resolution allowed it, the data was averaged to hourly means before comparison, otherwise daily medians were used. Gas concentration data was averaged from samples between 4.2 and 125 m, particle measurements are from ca. 4 m height. We emphasize that these data were not used as input in the model, instead the model relies completely on gridded, global emission, concentration and meteorological reanalysis data.

3 Results

3.1.1 Comparison of modelled and measured gas concentrations

The modelled and measured gas concentrations were aggregated to daily median gas concentrations at SMEAR II and are shown in Fig. 2, while the 8 months and summer medians are shown in Table 3. To obtain data that represents boundary layer at and just above the canopy, the hourly modelled values were obtained my taking the average between 8–50 m. The best model performance in terms of correlation during the 8 month period is seen in (r^2 and B_{NMBF} given in brackets) [acetone] (0.73, –1.95), [methanol] (0.67,–0.06), [monoterpenes] (0.59, –0.76) and [HOM] (0.53, 0.59), whereas smallest B_{NMBF} is seen in [methanol] and [O_3], with [HOM] and [monoterpenes] as distant 3rd and 4th. Worst performers in terms of correlation of daily medians were [H_2SO_4] (0.01, 2.33), [CO] (0.12, –4.21), [O_3] (0.10, –0.09, even though ozone is directly read in from CAMS) and [S_{O2}] (0.08, 2.10). Isoprene (0.52, –3.18) concentrations are underestimated quite substantially outside the growth season, whereas the discrepancy is smaller during summertime. The model overshoots [SO_2] and consequently [H_2SO_4], even when the SO_2 emissions were reduced by half. Ammonia is not routinely measured at SMEAR II, and the modelled [NH_3] is shown against weekly filter measurements available at EBAS database (https://ebas-data.nilu.no, last access Jan 31, 2025, Tørseth et al., 2012), which the model overshoots by an order of magnitude. As dry and wet deposition are the most significant sink for NH_3 and oxidation being negligible (Renard et al., 2004; Behera et al., 2013), the simplistic deposition scheme used here could result in accumulation along the trajectory. This means that the cluster formation in the ACDC could be enhanced towards the end of the trajectory by approximately a factor of 3 when compared to measured NH_3 concentrations (in STP, 10^7 cm^{-3} H_2SO_4 and 0.1–10 ppb NH_3 the formation rates vary between 1–4 cm^{-3} s^{-1}) Otherwise this overshooting has little effect in the model since the gas phase chemistry scheme does not have reactions involving NH_3, and the particle phase uptake of it in the model is limited by H_2SO_4 and HNO_3. Furthermore, the increased cluster formation (which is also due to likely overestimation of H_2SO_4) counterbalances the very conservative estimation of the DLPNO-based cluster chemistry.

https://doi.org/10.5194/egusphere-2025-39
Preprint. Discussion started: 7 January 2025
© Author(s) 2025. CC BY 4.0 License.

Modelled daytime median OH concentrations were on average 10^6 molecules cm^{-3} (the 95 percentile of daily concentrations were typically at 2–3×10^6 molecules cm^{-3}). Long-term OH measurements are not available for the time period, but the result can be compared with earlier SOSAA-modelled concentrations at SMEAR II (Chen et al., 2021), where the modelled daily median concentrations during the time period ranged between 1×10^6 – 6×10^6 molecules cm^{-3}. However, in that study the modelled OH concentrations were compared with measured concentrations during two earlier campaigns (EUCAARI, from late Apr–May 2007, Kulmala et al., 2011; Williams et al., 2011), and the model overestimated the measured daily median concentrations, which were consistently below 10^6 molec cm^{-3}. The authors discuss that the measurement height could affect the biases (the measurements were sampled close to the ground, typically at 4 m height, inside forest canopy). In our work the mixing inside and outside the canopy was not modelled in the same detail, and the difference between the first 10 m and the mean value between 10–80 m is negligible.

Similarly to OH, NO_3 measurements were unavailable, but our results with median night time [NO_3] of 8.6×10^6 molec cm^{-3} are somewhat higher than a previous modelling study from SMEAR II, which showed median nighttime concentrations of 4×10^6 molecules cm^{-3} for the year 2018 (Chen et al., 2021).

At SMEAR II the HOM are primarily products of monoterpenes (Ehn et al., 2014; Bianchi et al., 2019) and sesquiterpenes (Li et al., 2021; Dada et al., 2023). The lifetime of both terpenes and their oxidation products are short compared to the timescales of long-distance transport. Therefore, the good agreement with the modelled and measured [HOM] suggests that the emissions close to the station and the relevant chemistry are consistent with each other. These processes are vital steps in modelling SOA formation, and the results suggest that the model has the potential to describe SOA formation properly also upstream along the trajectories, given that the emissions are realistic. The biogenic emissions in CAMS are provided as monthly mean values, together with their mean daily profiles, and therefore are missing much of the day-to-day variation, and so will SOSAA. The modelling community would benefit from an open-access dataset with the gridded global modelled biogenic emissions from MEGAN (or any BVOC emission model) at high temporal resolution.

https://doi.org/10.5194/egusphere-2025-39
Preprint. Discussion started: 7 January 2025
© Author(s) 2025. CC BY 4.0 License.

Table 3: Median concentrations (molecules cm⁻³) of key components during summer (JJA) and total time period (Mar–Oct 2018), and bias (B_{NMBF}) between model and measured daily medians. Bias values in bold if FAC2>0.5.

	2018 Mar-Oct median (molec cm⁻³)			2018 Summer median (molec cm⁻³)		
	SMEAR II	**SOSAA-FP**	**B_{NMBF}**	**SMEAR II**	**SOSAA-FP**	**B_{NMBF}**
OH day		9.92×10^{5}			1.03×10^{6}	
OH night		5.32×10^{4}			9.45×10^{4}	
O_3	8.55×10^{11}	8.29×10^{11}	**–0.09**	8.09×10^{11}	8.85×10^{11}	**0.06**
NO_X	1.18×10^{10}	6.40×10^{9}	–0.97	8.28×10^{9}	6.37×10^{9}	**–0.24**
NO_3 day		1.73×10^{6}			1.81×10^{6}	
NO_3 night		8.61×10^{6}			6.89×10^{6}	
NH_3		3.96×10^{10}			3.58×10^{10}	
SO_2	1.10×10^{9}	5.01×10^{9}	2.18	1.05×10^{9}	4.39×10^{9}	3.49
H_2SO_4	2.86×10^{5}	1.24×10^{6}	2.32	4.81×10^{5}	1.36×10^{6}	2.39
Methanol	4.11×10^{10}	4.57×10^{10}	**–0.06**	8.13×10^{10}	8.17×10^{10}	**0.03**
Acetaldehyde	8.08×10^{9}	2.680×10^{9}	–2.01	1.03×10^{10}	3.01×10^{9}	–2.69
Acetone	2.94×10^{10}	1.13×10^{10}	–1.95	4.59×10^{10}	1.77×10^{10}	–2.02
Monoterpenes	4.61×10^{9}	3.19×10^{9}	**–0.77**	8.93×10^{9}	6.06×10^{9}	**–0.74**
HOM	5.50×10^{7}	7.66×10^{7}	**0.58**	1.11×10^{8}	1.44×10^{8}	**0.67**
Isoprene	2.12×10^{9}	2.75×10^{8}	–3.18	4.62×10^{9}	1.12×10^{9}	-2.86
Benzene	1.41×10^{9}	5.25×10^{8}	–1.21	8.71×10^{8}	3.48×10^{8}	–0.93
Toluene	2.38×10^{9}	2.52×10^{8}	–8.19	3.67×10^{9}	2.54×10^{8}	-14.3
CO	3.44×10^{12}	6.32×10^{11}	–4.20	2.87×10^{12}	7.63×10^{11}	-2.59

https://doi.org/10.5194/egusphere-2025-39
Preprint. Discussion started: 7 January 2025
© Author(s) 2025. CC BY 4.0 License.

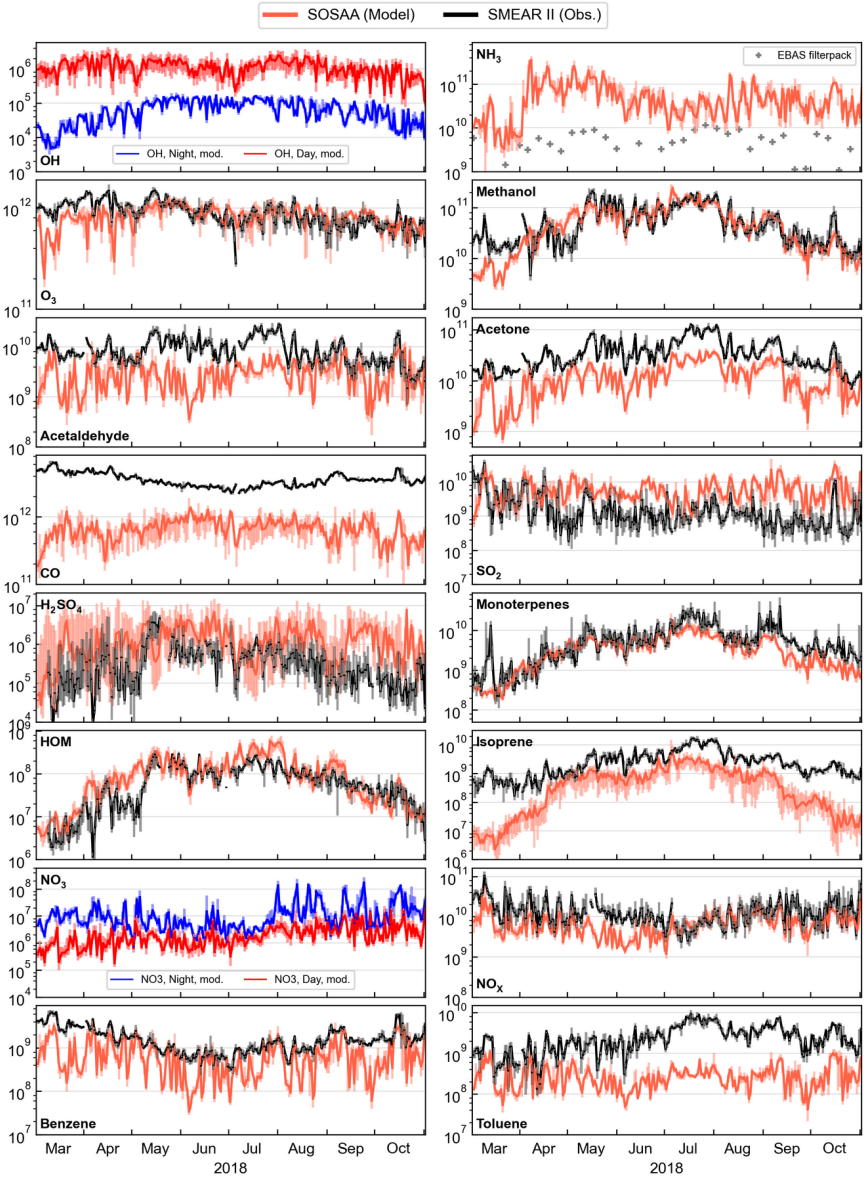

Figure 2: Daily median gas concentrations (cm^{-3}) at the SMEAR II station in the SOSAA model (red) and measurements (black) in the study period Mar–Oct 2018, with shaded ranges showing the interquartiles (25^{th} to 75^{th} percentiles of the data). The names of the compounds are shown in the corresponding panels. There are no measurements of OH and NO_3 from this time period, and for these compounds the modelled daytime (red) and nighttime (blue) values are shown separately. Note than O_3 concentrations are not modelled by SOSAA, but instead are read directly from CAMS. NH_3 measurements (shown with grey markers) come from EBAS filter measurements with 1 week time resolution.

https://doi.org/10.5194/egusphere-2025-39
Preprint. Discussion started: 7 January 2025
© Author(s) 2025. CC BY 4.0 License.

425

3.1.2 Aerosol size distributions and composition

Figure 3 shows the modelled and observed particle size distributions at SMEAR II (panel a) and the size-resolved ratios between the two (panel b), so that the ratio E for bin i was defined as $E_i = \frac{N_{i,MOD}}{N_{i,OBS}}$. Figure 3b also shows on the right axis the time-averaged (12 days running mean) ratios for the comparable total size distribution 3–1000 nm and three subclasses; 3–30 nm, 30–100 nm and 100–1000 nm, approximately corresponding to nucleation, accumulation and coarse modes. The B_{NMBF} of the modelled number concentrations in total, nucleation, accumulation and coarse modes are –0.163, 0.793, –1.346 and –0.710, respectively, meaning the model on average produced more particles in nucleation mode and less in other modes, with clear exceptions in July and early September when the observations showed low concentrations in the nucleation mode while the mode was practically absent in the model. This period has been discussed in earlier studies where the July heat wave resulted in decreased gross primary production in large parts of central and north-western Europe, when compared with earlier years. Heikkinen et al. (2020) report a high SOA loading in July, but also an increased anthropogenic organic component in PM_1. We attribute the weak new particle formation in the model to elevated temperatures and condensation sink due to primary emissions upstream of the trajectories (Fig. 11), which effectively reduces cluster formation in the ACDC module (Fig. S4–S6). The increased particle number emissions along the trajectory in mid-July to early August coincide with the decreased nucleation rates in the model. While the number emissions especially 3 days prior to arriving at station were among the highest in the period, similar emissions were observed in March, but with much less nucleation inhibition, which could partly be explained by the lower temperatures. Other factors such as NH_3 and SO_2 emissions along the trajectories did not markedly differ in July from adjacent months (Fig. S8).

445

https://doi.org/10.5194/egusphere-2025-39
Preprint. Discussion started: 7 January 2025
© Author(s) 2025. CC BY 4.0 License.

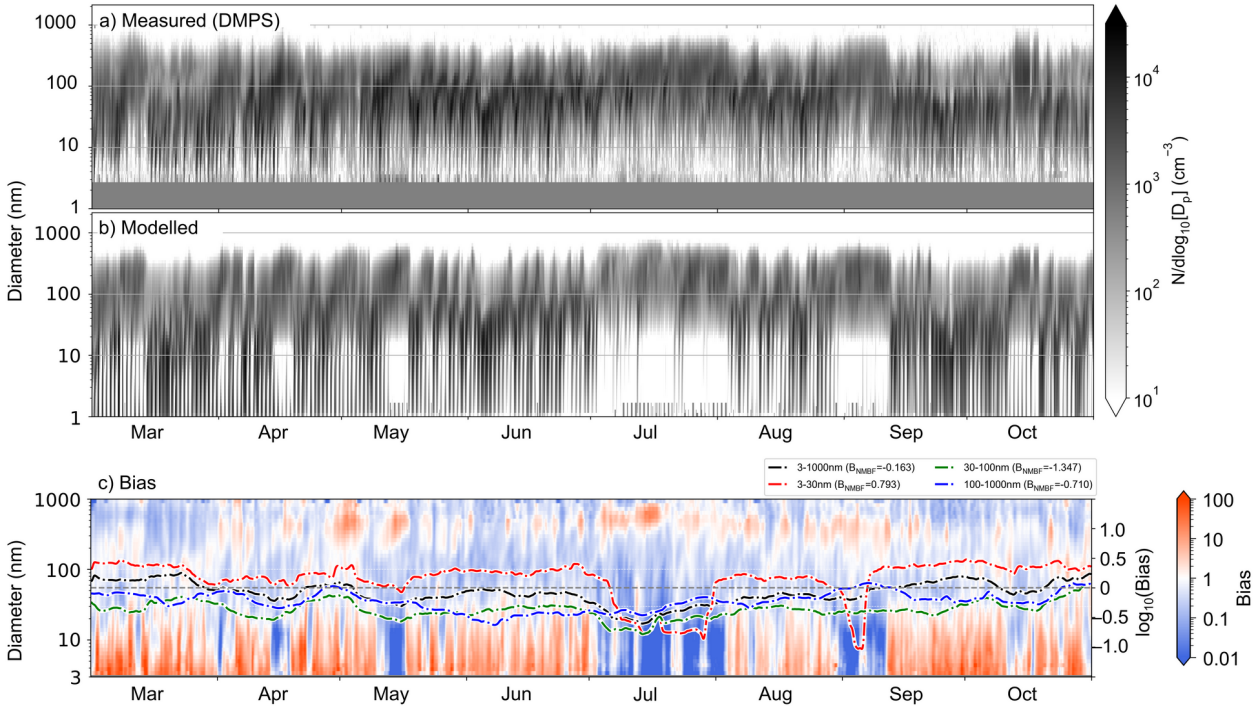

Figure 3: a) Measured (with DMPS) and b) modelled particle size distributions from the study period. c) Model bias as ratio of model and measurement (Model/Measurement). Heatmap shows the size distribution of the bias; black, red, green and blue dashed lines show a 12-day running bias for 3–1000 nm, 3–30 nm (nucleation mode), 30–100 nm (Aitken mode) and 100–1000 nm (accumulation mode), respectively. The legend shows the normalized mean bias factor (B_{NMBF}) for the total time period for the selected size classes.

The lower sensitivity of the DMPS instrument (well below 10 nm) can explain only a small fraction of the overshooting in the smallest sizes, and therefore it is possible that the model bias is due to insufficient growth of the nucleation mode, leading to underestimation of the larger particles. Possible reasons for this could be a significant underestimation of the concentrations of extremely low-volatility organic compounds (ELVOC), overestimation of the saturation vapour pressures of the current vapours, missing particle phase reactions which could decrease volatility of organic compounds and thus reduce their later evaporation, missing cloud processing or insufficient partitioning of inorganic compounds. The perturbation run Sensi-BIO (Table 2) saw the size distribution shifting towards larger sizes (especially noticeable in June, see Fig. S9). However, the gas phase [HOMs] were relatively well captured in the BASE, and the particulate ammonium and nitric acid were already overestimated when compared with ACSM measurement. This leaves the cloud processes or particle phase reactions as possible additions to the model which could reduce the difference in the modelled and measured size distributions. Whether either of these would markedly shift the nucleation mode, which is well beyond activation size, and where SVOCs

https://doi.org/10.5194/egusphere-2025-39
Preprint. Discussion started: 7 January 2025
© Author(s) 2025. CC BY 4.0 License.

accumulate weakly, is unclear. Cloud droplets are a sink for the particles below activation size (Pierce et al., 2015), and this missing sink could partially explain the overestimation of the nucleation mode, although they might not be deposited in rain-out in case of cloud droplet evaporation.

Modelled aerosol mass composition was compared with ACSM measurements from SMEAR II. SOSAA stores detailed information of the secondary organic aerosol, but a substantial fraction of the aerosol loadings in the model comes from anthropogenic particle emissions, whose composition varies, and is not known in sufficient detail. Here we assumed that the PNE are primarily composed of organic compounds, black and brown carbon and sulfates. The ACSM shows organic aerosol, sulfates, nitrates, ammonium and chlorides, but cannot measure (refractive) black carbon. For Fig. 4 we attributed the modelled SOA and 85 % of the primary particle mass to organic aerosol, all sulfuric acid and the remaining 15 % of primary particle mass to sulfates, nitric acid to nitrates, particle phase ammonia to ammonium and 60 % of sea salt mass to chlorides. The majority of the measured and modelled particles are organics and sulfates. The model is able to capture the time series of the total mass to a good degree; for the 24 h running mean B_{NMBF}: 0.17 (r^2: 0.53), and by component OA: 0.01 (r^2: 0.70), SO_4: –0.40 (r^2: 0.40), NO_3: 2.05 (r^2: 0.31), NH_4: –0.22 (r^2: 0.45), Cl: –0.17 (r^2: 0.02). For the sum OA+SO_4 the B_{NMBF} was 0.04 (r^2: 0.62).

https://doi.org/10.5194/egusphere-2025-39
Preprint. Discussion started: 7 January 2025
© Author(s) 2025. CC BY 4.0 License.

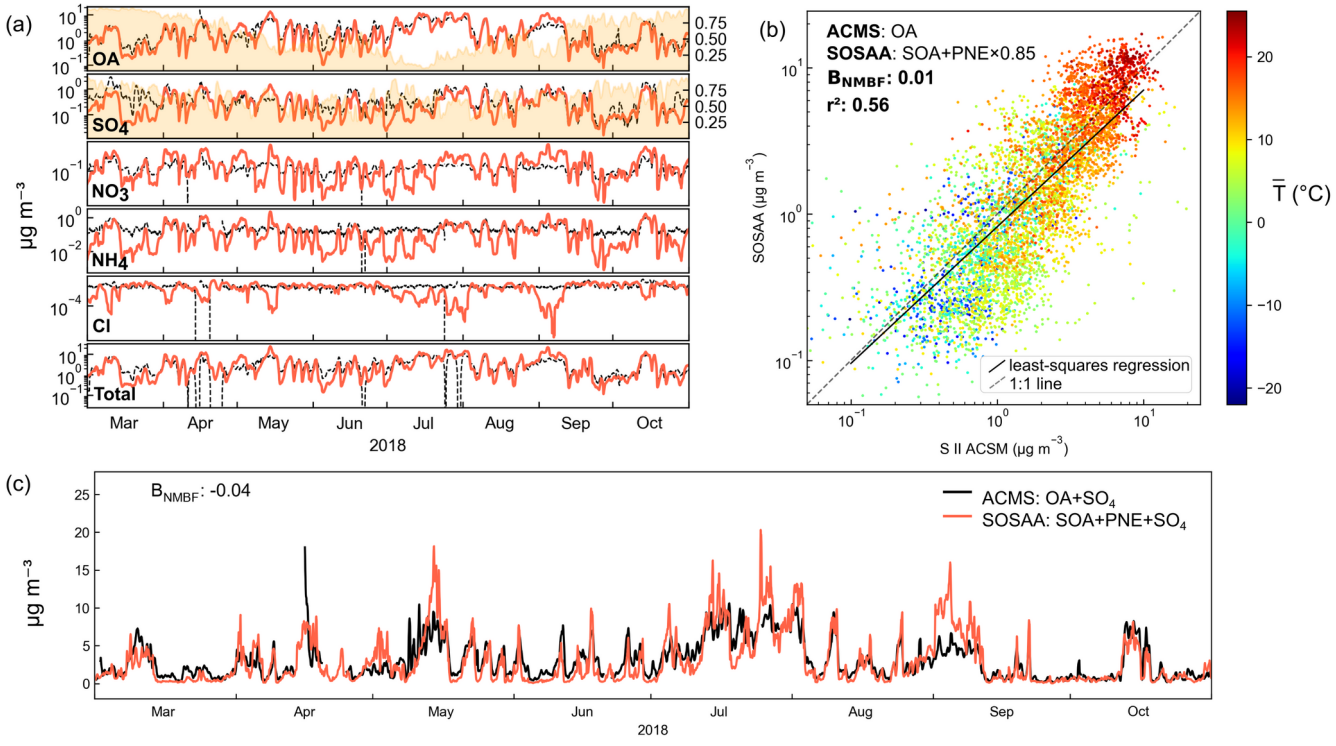

Figure 4: Panel (a): 24-hour running mean of mass composition from ACSM measurements with component labels in the lower left corners of the subplots. For this figure 85 % of the primarily emitted particle (PNE) mass in the model was attributed to organic aerosol (OA), and 15 % to sulfates (SO_4). The yellow shading with the axis on the right shows the modelled mass fraction coming from the primary particles. Panel (b): The scatter plot of 3-hourly values organic aerosol of PM_1 from ACSM and SOSAA (obtained similarly as in in panel (a), coloured with mean temperature during the last 4 days along the mean trajectory. Panel (c): The unfiltered 3-hourly ACSM OA+SO_4 and SOSAA PNE + SOA + SO_4.

Figure 5 shows the size-resolved relative fractions of the particle composition in the SOSAA model. The secondary aerosol mass is the dominant fraction in the 1–10 nm range (around 80 % of mass) and comprises more than 60 % of the mass in the 10–100 nm diameter range, especially in the summer months when the secondary mass is on average between 65 % to 85 % of the total mass in the size range. For sizes over 200 nm in diameter, primary emissions start to dominate the mass, with a tail of sea salt from approximately 500 nm diameter upwards. Figure 6 shows that episodes with elevated PM_1 concentration can occur with very different contributions of primary, secondary organic and secondary inorganic aerosols. This is evident, e.g., in the episodes when PM_1 exceeds 8 µg m^{-3} for several days: during those in Mar–Apr and in Sep–Oct, the composition

https://doi.org/10.5194/egusphere-2025-39
Preprint. Discussion started: 7 January 2025
© Author(s) 2025. CC BY 4.0 License.

is mostly primary and inorganic secondary aerosol; during those in Apr–May and August, SOA slightly exceeds primary and secondary inorganic contributions; and during the Jun–Jul episode, SOA clearly dominates PM_1 mass. Measurements of size resolved aerosol composition from SMEAR II station exist from March–April 2003, where days with cleaner northern air (associated with higher likelihood of new particle formation events) showed high fraction of organic mass from terpene oxidation products in nucleation and Aitken modes, and organics, nitrates and sulfates in the accumulation modes (Allan et al., 2006). Another related study used Nano Aerosol Mass Spectrometer (NAMS) to measure the composition of particles between 15 and 22 nm in diameter at SMEAR II in March–April 2011, and reported molar fractions of sulfur (7 %), nitrogen (14 %), carbon (38 %) and oxygen (45 %) during 8 NPF event days (Pennington et al., 2013). Similar analysis from our data during daytime (06–18) MAM showed 2 %, 13 %, 35 % and 50 % molar fractions of sulfur, nitrogen, carbon and oxygen, respectively (calculated with 1:1 C:O mass fraction in OA). While our results agree with these studies, their short time period and long time difference makes more detailed quantitative comparison impractical.

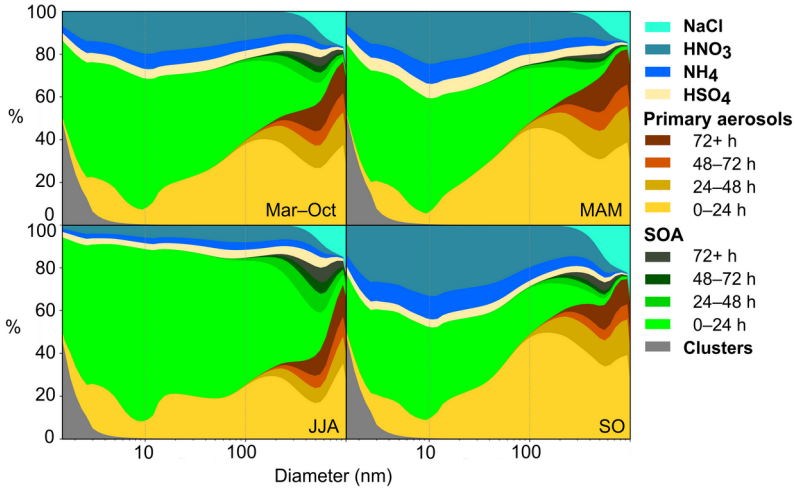

Figure 5: Modelled, size dependent aerosol mass fractions of aerosol components for the the whole period (Mar–Oct), spring (MAM), summer (JJA), and autumn months (SO). "Primary aerosols" refers to particles that originate from anthropogenic particle emissions (PNE), SOA refers to organic aerosol that has formed through condensation of vapours. Primary particles and SOA are classified by their age in the final PSD; age refers to the time since they were emitted or formed in the model.

https://doi.org/10.5194/egusphere-2025-39
Preprint. Discussion started: 7 January 2025
© Author(s) 2025. CC BY 4.0 License.

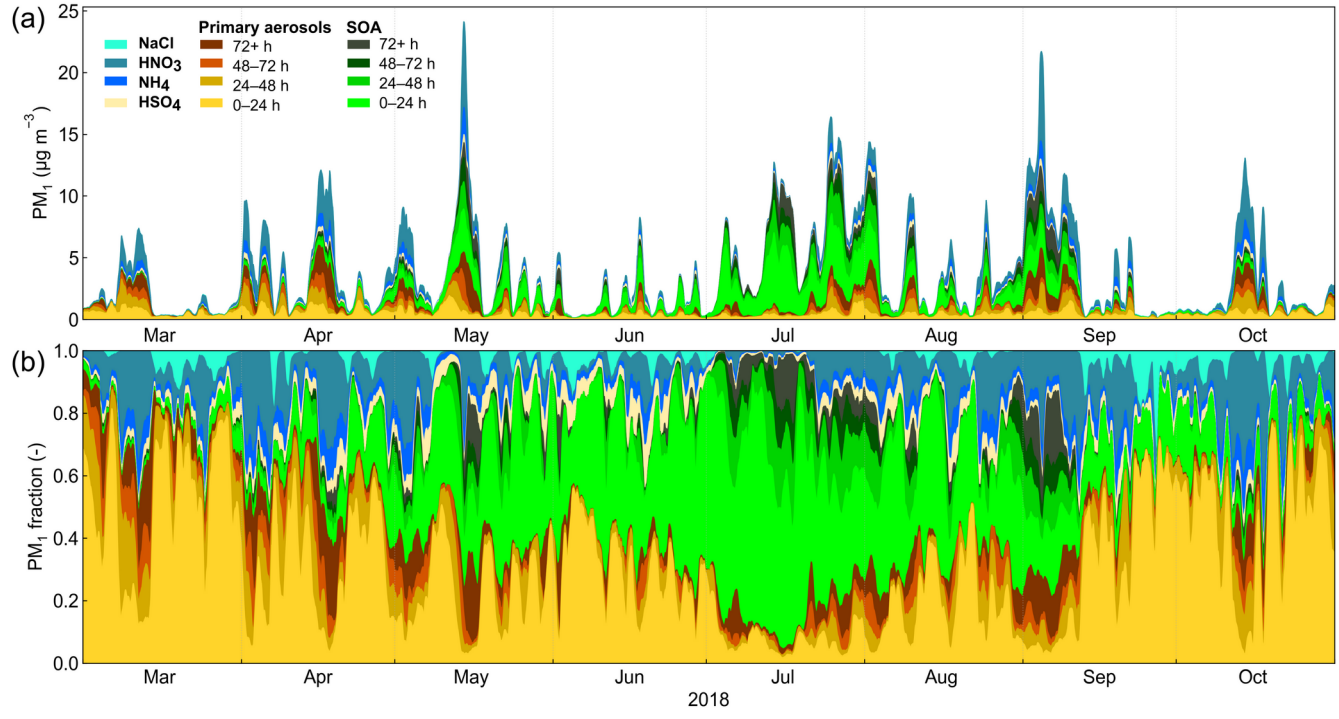

Figure 6: (a) Time series of modelled PM_1 aerosol components. (b) Modelled PM_1 aerosol component mass fractions. Data is shown as moving average (24-hour boxcar) of hourly values. PNE refers to particles that originate from anthropogenic emissions, SOA refers to organic aerosol that has formed through condensation of vapours.

3.1.3 CCN concentrations

Figure 7 shows model and SMEAR II measurements of CCN, for three maximum supersaturations. The measured 8-month time series shows large variation, generally higher median concentrations in the summer months and lower in the two autumn months. Summertime (JJA) median of measured [$CCN_{0.5\%}$] was approximately +28 % of the 8-month median, autumn (SO) approximately –60 % of total median concentration, spring (MAM) being close to total median. In the 0.1 % supersaturation class only autumn concentrations differed significantly (–40 %, $p<0.01$) from the total median. The model underestimates the concentrations of the 0.2 % and 0.5 % supersaturation classes, and overestimates the 0.1 % class, and does not capture the statistically significant increase in the summertime in the larger supersaturation class but does so with the autumn decrease. The modelled median [CCN] in the supersaturations above 0.5 % showed practically no change in the summertime

https://doi.org/10.5194/egusphere-2025-39
Preprint. Discussion started: 7 January 2025
© Author(s) 2025. CC BY 4.0 License.

and only a weak, statistically insignificant decrease in the autumn. As the measurements for the time period were available only for up to 0.5 % supersaturation, this cannot be verified against observations, but it seems reasonable to assume that the same trends that were observed in the 0.5 % supersaturation class would continue even in smaller particles. Figure 8 shows that although the model is able to capture the variation in [CCN] in short time scales, as evident from the satisfactory correlation of the daily median in all compared supersaturation classes (r^2 was 0.49, 0.61 and 0.58 for 0.5 %, 0.2 % and 0.1 % supersaturation [CCN], respectively), the seasonal dynamics of [CCN] remained elusive and the increase in the summertime smaller diameter [CCN] is missed. In [$CCN_{0.1\%}$] the model has least bias in the summer months, which could be an indication that the coarse mode particles (from primary emissions) are overshooting, and, as they are sinks to smallest particles, this would lead to underestimation of the higher supersaturation classes. However, the time series shows that during the same periods when the model overestimates [$CCN_{0.1\%}$], the other classes have very little bias (spring) or increase their overestimation (Aug–Sept). In general both modelled and measured [CCN] correlate with primary emissions – r^2 between mean PNE 0–4 days before the station and [$CCN_{0.1\%}$] at the station was 0.57 for modelled and 0.38 for measured CCN; same comparison for [$CCN_{0.5\%}$] showed r^2 of 0.34 and 0.21 for modelled and measured CCN, respectively.

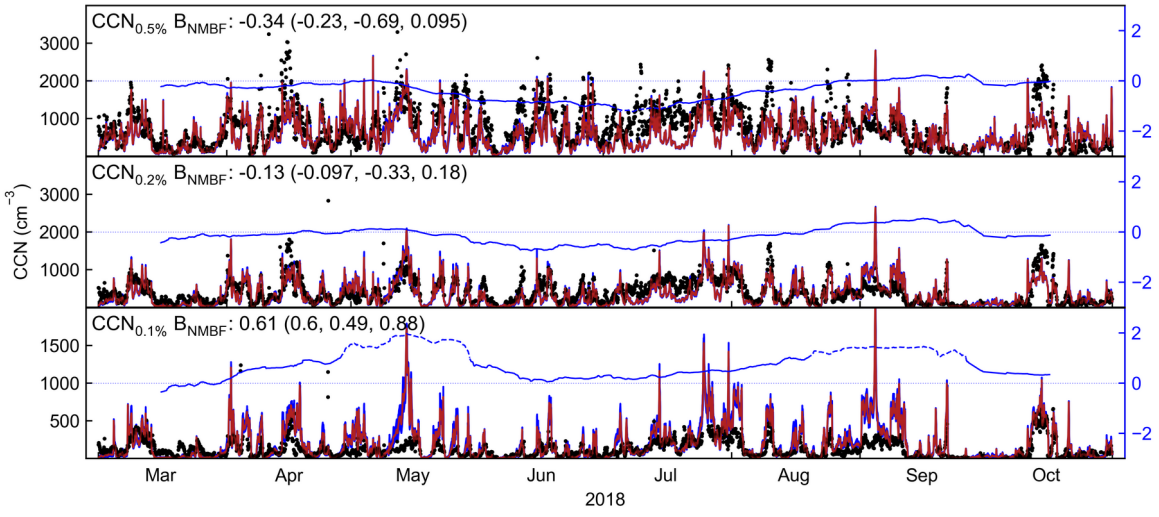

Figure 7: Measured (black markers) and modelled (red line) CCN number concentration for 0.5 %, 0.2 % and 0.1 % supersaturation. A blue shading is shown along the modelled [CCN] where the concentrations are calculated using the upper and lower limits of the κ-values of the components (see Table S2), giving an estimate of the uncertainty that is related to the component activities. For the most part the uncertainty due to κ is too small to stand out from the figure. The axis on the right shows the running B_{NMBF}, with 30-day window, solid line marks periods where model is within a factor of two of measurements ($|B_{NMBF}|<1$).

https://doi.org/10.5194/egusphere-2025-39
Preprint. Discussion started: 7 January 2025
© Author(s) 2025. CC BY 4.0 License.

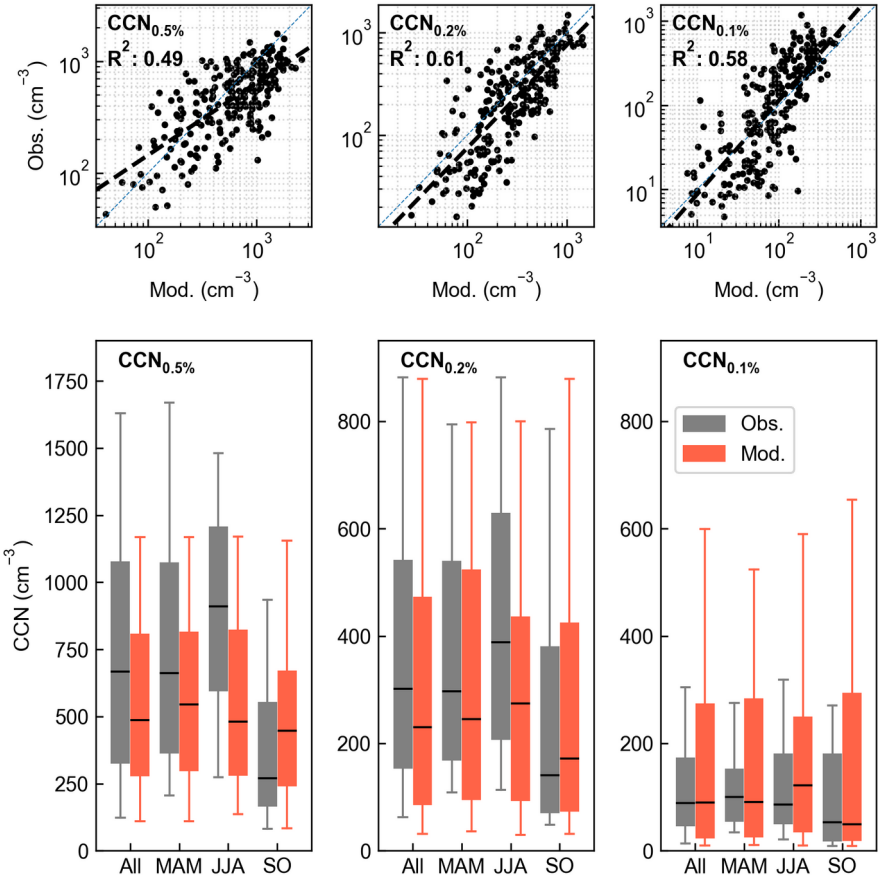

Figure 8: Scatter (top row) and box plots (bottom row) of modelled and measured daily median CCN number concentrations of three supersaturation classes (left column: $CCN_{0.5\%}$; middle column: $CCN_{0.2\%}$; right column: $CCN_{0.1\%}$). Box plots show data for full period (All), spring (MAM), summer (JJA) and the early autumn (SO), boxes include 25–75 percentiles, while whiskers show 5–95% range. Note the different scales in each supersaturation class.

3.2 Model sensitivity: CCN response to selected parameters

The model has shown good potential in capturing the variability of local gas concentrations as well as particle concentrations and composition, including CCN concentrations. The following sensitivity tests investigate the model response (R) to changes in some key parameters. Figure 9 shows the responses of three CCN supersaturation classes (1.0 %, 0.4 % and 0.2 % maximum supersaturation) to the perturbations in the three "Sensi" runs (see Table 2). In all classes, the model CCN are generally most responsive to the primary particle emissions, followed by BVOC emissions, whereas changes in cluster formation rates show the least response. However, the responses show large variation in seasonal and synoptic time scales, which could relate to the seasonal variation of BVOC emissions, as well as the history of the trajectories, namely which geo-

https://doi.org/10.5194/egusphere-2025-39
Preprint. Discussion started: 7 January 2025
© Author(s) 2025. CC BY 4.0 License.

graphical areas and conditions (meteorological, emissions) they originate from (discussed in Sect. 3.3). The distributions of the responses, shown on the right panels in Fig. 9, show that all parameters have, on average, mostly a positive impact – that is – increasing the variable increases CCN concentrations. However, all parameters occasionally show negative responses, meaning that an increase will decrease CCN concentrations. This is most evident in the case of cluster formation rates, where for the lowest maximum supersaturation (largest diameter particles), increased nucleation rates show a negative response in CCN concentration, although the effect is much smaller in either direction than those of PNE or BVOC emissions. This is in line with some modelling studies where high concentrations in the nucleation mode caused a decrease in low volatility vapour concentrations and hindered the growth of larger particle sizes, resulting in less CCN in the lower supersaturation range (Roldin et al., 2019; Patoulias et al., 2024). Cluster formation rates have a positive but surprisingly small effect to higher maximum supersaturation (smaller diameter) CCN. The R_{NUC} stays in general below 10 % (8 % for the exponential effect $R_{NUC,POW}$), meaning that to approximately double the CCN concentrations, more than ten-fold increase in the formation rates is needed, whereas a ten-fold decrease would decrease CCN by less than 10 %. The diurnal profiles of the responses reveal a more detailed picture where daytime CCN concentrations show considerably higher sensitivity to cluster formation rates, and lower to particle number emissions, when compared with the seasonal medians (Fig. S19). Changes in BVOC emissions affect CCN in a similar, if more benign, diurnal pattern as changes in PNE. It is not immediately clear how to interpret this behaviour, but during summer months when emissions peak the response is strongest in the lowest supersaturation class, which at least implies that the effect of BVOC emission is particularly affecting the particles that are in the upper range of the Aitken mode, able to accumulate mass via compounds that are low- or semi-volatile, as opposed to extremely low volatility vapours. This would favour the primary particles, which are already in this size range upon emission.

https://doi.org/10.5194/egusphere-2025-39
Preprint. Discussion started: 7 January 2025
© Author(s) 2025. CC BY 4.0 License.

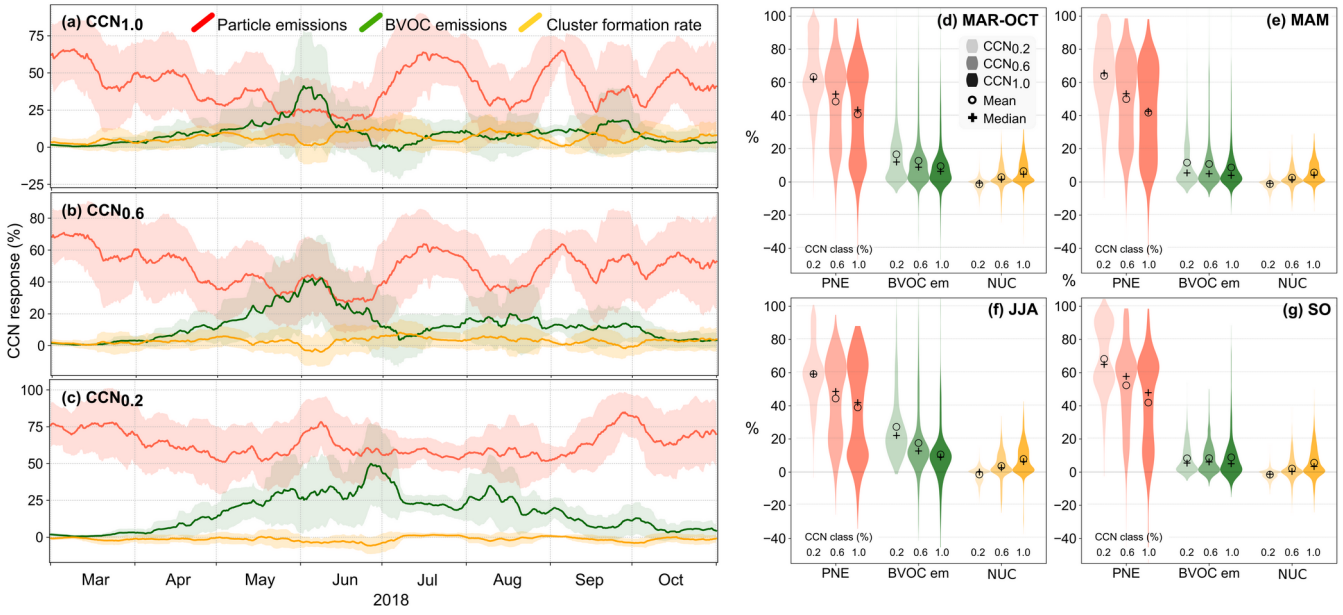

Figure 9: The calculated responses R_{PNE}, R_{BIO} and R_{NUC} of CCN number concentration to changes in anthropogenic particle emissions (red), BVOC emissions (green) and cluster formation rate (yellow), shown as 12-day running mean for three supersaturation classes: a) 1.0 %, b) 0.6 % c) 0.2 %. The input parameters were varied separately in the three "Sensi"-simulations (Table 2). The shaded areas show the ± standard deviation for the 12-day window used in the running mean. Panels d–g show the grouped distribution of the responses in a–c as violin plots for the full study period (d), spring (e), summer (f) and autumn (g), with mean marked with circle and median marked with cross.

Figure 10 shows the differences in median CCN concentrations between Zero-simulations (Table 2) and BASE for the total dataset, separated to daily, daytime and nighttime medians (the monthly distributions of the changes, along with 12-day running mean are shown in Fig. S18). Setting the formation rates to zero changed the median [$CCN_{1.2\%}$] by –48 % (–50 %,–45 %) and median [$CCN_{0.1\%}$] by +23 (+12 %,+35 %), where range in brackets is the 95 % confidence interval of the change obtained by random sampling of the Zero-simulation distributions ('bootstrapping'). Monthly analysis shows that this increase was mostly due to increase in June and October, while in other months the median $CCN_{0.1\%}$ concentrations were not significantly different (Mood's test) from the BASE. However, due to the low [$CCN_{0.1\%}$] in June the strong increase was not in general reflected in the summertime median concentrations, which increased by only 14 % (Table S4). The large variation in the effect of cluster formation underpins the complex dynamics of the atmospheric particles and highlights the caveats of expressing the contribution of different processes in a single figure. Removing PNE from the model decreases the coagula-

https://doi.org/10.5194/egusphere-2025-39
Preprint. Discussion started: 7 January 2025
© Author(s) 2025. CC BY 4.0 License.

tion sink, thereby increasing the cluster formation rates (on average by approximately threefold), and these changes in ZeroPNE simulation are shown in Fig. S7 and further discussed in the Supplementary material.

Removing all particle emissions from the model had generally a decreasing effect in all CCN classes, strongest in the $CCN_{0.1\%}$, where the change in median concentrations was –82 % (–86 %,–78 %) and smallest in the $CCN_{1.2\%}$ class with a change of –33 % (–36 %,–29 %). As expected from the diurnal profiles of the responses, removing cluster formation had a stronger effect in daytime CCN concentrations, while the opposite was true for removing PNE (Fig. 10). The diurnal effect increased towards the smallest CCN sizes and was particularly evident in the ZeroPNE simulation, where the daytime decrease of median [$CCN_{1.2\%}$] (–19 %) was less than half of what was seen in nighttime concentrations (–46 %).

The results form the Zero-simulations, backed with the sensitivity studies, can be used to estimate the overall impact of new particle formation and primary number emissions to the CCN concentrations. The effects differ markedly in the extreme ends of the chosen supersaturation classes: The $CCN_{0.1\%}$ seems to be dominated by the primary emissions; we estimate 85 % of daytime and 90 % of nighttime concentrations of the study period and location can be attributed to PNE, while NPF contributes approximately 65 % of the daytime and 45 % of the nighttime $CCN_{1.2\%}$ concentrations. The seasonal and synoptic variability is considerable, and these fractions would differ markedly for specific time periods or seasons (Fig. S18). Therefore, these results underline the complexity of atmospheric particle formation, and further highlight the caveats of quantifying the impact of NPF without specifying the time of year, location, supersaturation class, particular metrological conditions, etc.

https://doi.org/10.5194/egusphere-2025-39
Preprint. Discussion started: 7 January 2025
© Author(s) 2025. CC BY 4.0 License.

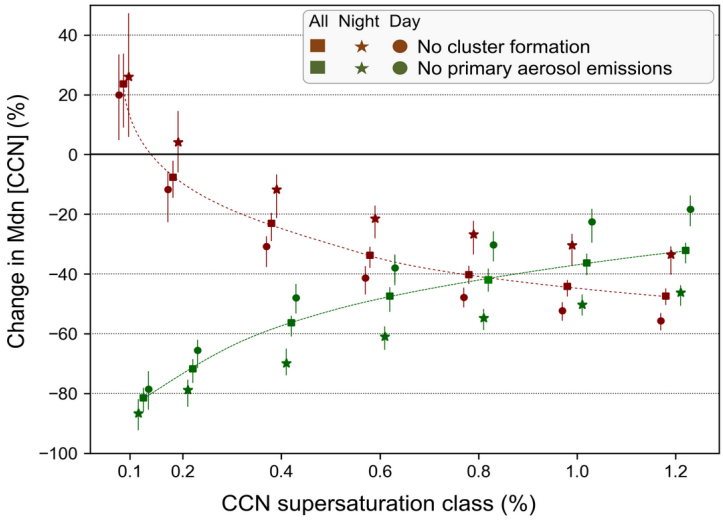

Figure 10: Relative change in median CCN number concentrations between Zero-simulations and BASE (Table 2), during the study period Mar–Oct, for nighttime (21–07 local time, marked with star symbol), daytime (08–20 local time, marked with round symbol) and daily concentrations (marked with squares). The vertical range represents 95 % confidence intervals of the median, obtained from bootstrapping. The spline fits for daily change of medians are provided for visual aid only.

575

3.3 Origins and history of modelled CCN

Figure 11 shows the geographical origins of the air masses as azimuths and straight line distance from the SMEAR II station for the last four days before arriving at the station, as well as some relevant model variables for CCN formation. For discussion, panel b also shows the modelled [$CCN_{0.2\%}$] and [$CCN_{1.0\%}$]. This overall view on the study period serves as a basis when
580 we try to identify the origins (both geographical and processes) that lead to CCN. In March, cluster formation rates were average throughout the period, with low BVOC emissions. Early March peak in CCN is accompanied with some BVOC and notable PNE and cluster formation, origins from south-east, whereas second half of March saw below average CCN, PNE and BVOC, with average cluster formation, and origins from north-westerly direction. With increasing temperatures in April the BVOC emissions pick up, cluster formation is strong, but the peaks in CCN coincide more with elevated PNE (and
585 BVOC). The end of April shows airmasses originating from west of SMEAR II, elevated cluster formation rates 3–4 days prior to station, followed by increasing BVOC emissions and decreasing particle emissions during the last two days. The resulting increase in [$CCN_{1.0\%}$] at the end of April could be a typical pathway from new particle formation to CCN, whereas the peak in mid-May, while still showing strong BVOC emissions, seems to mostly originate from PNE. Otherwise, much of the

https://doi.org/10.5194/egusphere-2025-39
Preprint. Discussion started: 7 January 2025
© Author(s) 2025. CC BY 4.0 License.

April–June period includes trajectories with westerly to north-westerly component, formation of clusters and average [$CCN_{1.0\%}$]. Especially in June primary emissions were low, cluster formation along trajectories generally lasted for days with BVOC emissions overlapping, indicating that much of the CCN was likely formed from NPF (as also indicated by the Zero-simulations). In contrast, July and early September mostly saw periods with weak cluster formation, elevated BVOC and primary particle emissions, related to south-easterly origins of the airmasses, coinciding with some of the highest CCN concentrations in the studied time period. The different pathways of CCN origins are also supported by the fractions of [$CCN_{0.2\%}$]/[$CCN_{1.2\%}$] (Fig. S16), where low fractions are seen in end of March, end of April, June, mid-August and late September and early October, coinciding with low PNE (and lower than average fraction of 3–30 nm emissions) and suggesting formation of CCN via NPF.

https://doi.org/10.5194/egusphere-2025-39
Preprint. Discussion started: 7 January 2025
© Author(s) 2025. CC BY 4.0 License.

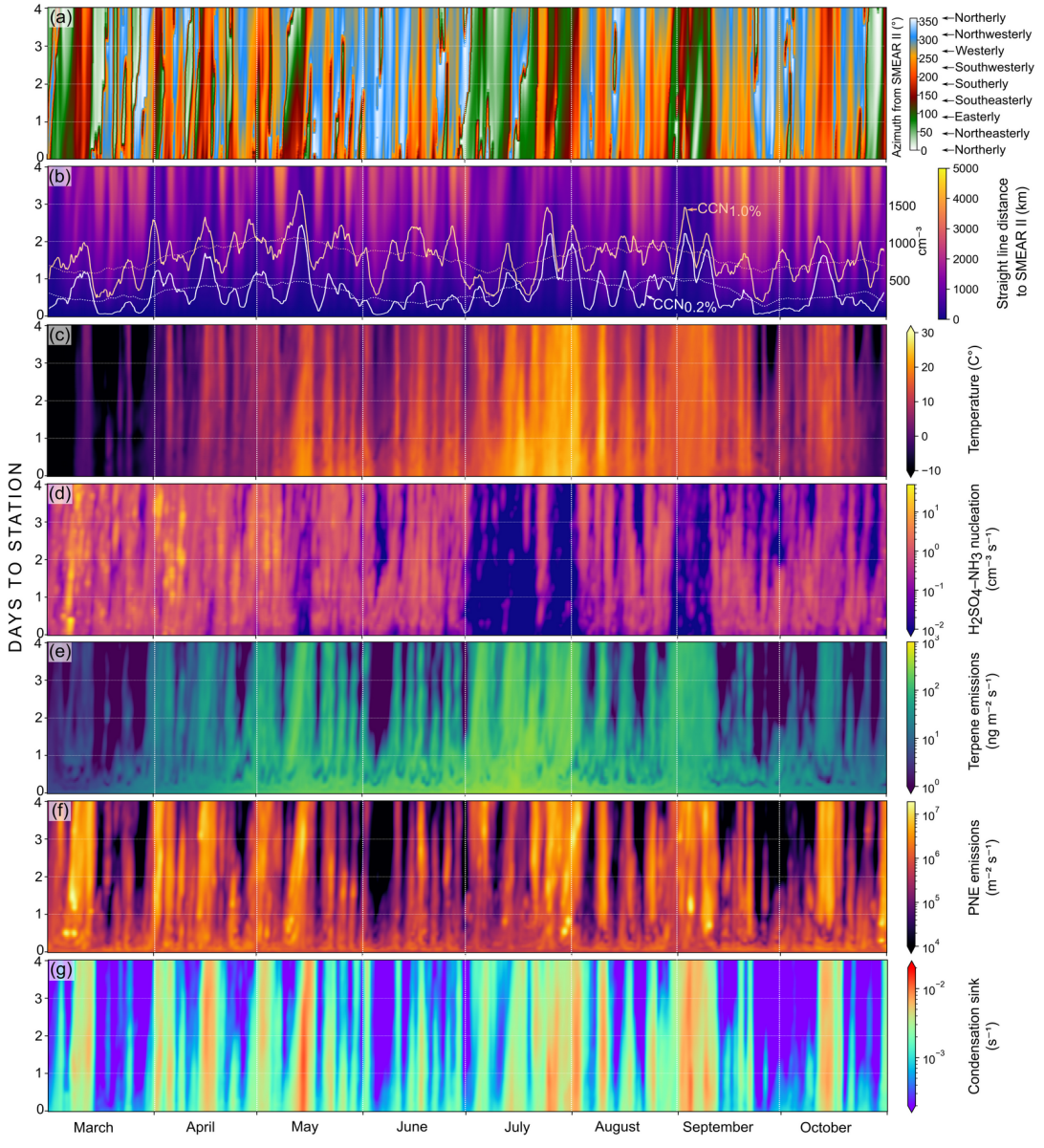

Figure 11: Hovmöller diagrams showing the 4-day history of the air masses and model parameters which are relevant to CCN formation. a) azimuth, i.e. bearing from SMEAR II; b) straight line distance (km) from the station to the trajectory mean, superimposed are the 30-day and 3-day running mean of modelled [$CCN_{0.2\%}$] and [$CCN_{1.0\%}$] at the station (right axis); c) temperatures (C°), note that the color scale only covers the range between –10°C and 30°C; d) formation rates from the ACDC H_2SO_4–NH_3 module; e) terpene (mono and sesquiterpenes) emissions; f) total primary anthropogenic particle number emissions; g) condensation sink of sulfuric acid, used as a scaling factor to estimate coagulation losses of interstitial mo-

https://doi.org/10.5194/egusphere-2025-39
Preprint. Discussion started: 7 January 2025
© Author(s) 2025. CC BY 4.0 License.

lecular clusters in the ACDC module. 1-hour resolution data is filtered with a 12-hour gaussian kernel on the horizontal, and unfiltered on the vertical dimension.

Figure 12 shows the geographical origins of the airmasses in the summer (June–August), illustrated with the density of the FLEXPART Source-Receptor Relationship (SRR) values, grouped in sectors where each sector is 1000 km further away from the SMEAR II station. For clarity, the first 200 km radius is left out as the direction of advection at the station is not relevant in this context. The trajectories were divided in two groups, where the top (bottom) row is an aggregation of the trajectories that showed above (below) median CCN 0.4 %. For the most part the above median CCN trajectories showed high SOA and primary particle mass. The below median trajectories show the typical origins that favor NPF events, while the above median trajectories have a southerly component, favouring BVOC but also anthropogenic emissions, although 3–4 days prior to station the airmasses are quite dispersed and also show some NPF favoured North-Westerly component.

https://doi.org/10.5194/egusphere-2025-39
Preprint. Discussion started: 7 January 2025
© Author(s) 2025. CC BY 4.0 License.

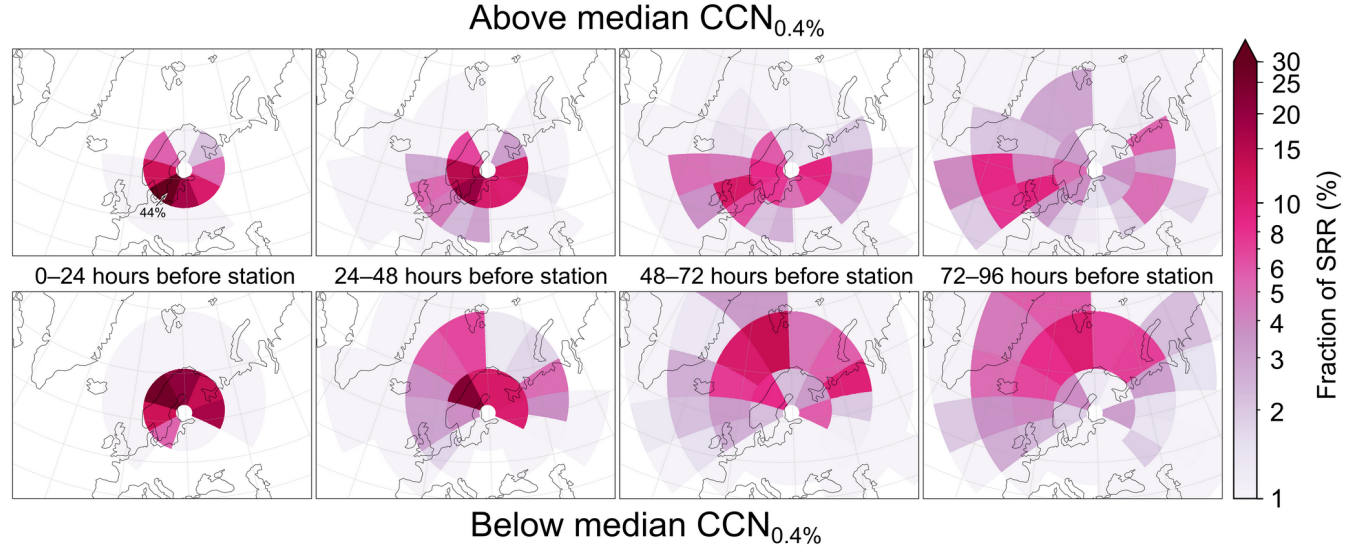

Figure 12: Locations of summertime (JJA) airmasses 0–4 days prior to arriving at the SMEAR II, based on the FLEXPART Source-Receptor Relationship (SRR) distribution. The aggregated SRR data were divided by the modelled [$CCN_{0.4\%}$] so that top row shows trajectories which showed more than JJA median, and bottom row trajectories whose [CCN] was below JJA median. The radial distance of each sector edge is 1000 km further from the previous (the traces within innermost 200 km radius from SMEAR II station were omitted from the calculation). Note that the colour scaling is logarithmic (fraction is shown on the map if it exceeds the scale).

4 Discussion and Conclusions

In this work we have used a novel Lagrangian modelling framework to examine the origins and history of gas and aerosol components observed at the boreal forest measurements site SMEAR II. This framework utilizes global emission datasets, backward trajectories from FLEXPART model, and a detailed description of atmospheric chemistry and aerosol dynamics from SOSAA model. We have applied this SOSAA-FP framework to simulate a period from March to October 2018 with one hour time resolution. The framework simplifies the three-dimensional transport of atmospheric components and in turn provides a much richer description of gas-phase chemistry, aerosol dynamics and composition than a large scale 3-D model would. Model and observation comparison showed that the framework enables assessments of the impacts of airmass ori-

https://doi.org/10.5194/egusphere-2025-39
Preprint. Discussion started: 7 January 2025
© Author(s) 2025. CC BY 4.0 License.

gins, emissions, meteorology, and seasonal variations. The results are particularly promising for larger aerosol particles, where bulk particulate mass, composition, and CCN activity are well modelled. Challenges persist in capturing the size distributions of smaller particles and certain gas-phase species, although these challenges are also related to the input data. Despite the limitations, SOSAA shows great promise for future applications in fields such as air quality, cloud formation, and aerosol optics.

Sensitivity experiments show that CCN concentrations are highly sensitive to primary particle emissions, especially outside the growing season. Accurate estimates of size-dependent primary particle emissions are crucial, as they strongly impact CCN concentrations and aerosol size distributions. During summertime, the influence of BVOC emissions on CCN concentrations is comparable to that of primary aerosols but diminishes again outside the growing season, as expected in northern latitudes. Although winter months were excluded from the study, it seems plausible that primary particle emissions (PNE) remain the most influential during periods of higher energy consumption and low BVOC emissions. The summertime CCN sensitivity to BVOC emissions was highest in the largest CCN sizes, which is likely explained by the volatility distribution of the oxidation products; larger particles will act as a sink to a certain fraction of vapours, while only a smaller subset of low volatility vapours will condense on the smallest particles.

Increased atmospheric cluster formation has little or negative impact on the smallest supersaturation CCN number concentrations but the effect becomes positive at higher supersaturation classes. However, this effect is smaller on average than the effects of changes in BVOC or primary particle emissions, and show a strong diurnal pattern (opposite profile to PNE). Daytime responses to cluster formation in the smallest CCN sizes are comparable to, or even exceed those of BVOC emissions, but are still less than half of the response to PNE. The analysis of ZERO-simulations suggests that the effect of cluster formation on CCN concentrations can be approximated with a power law, where the factor of change of CCN is proportional to the change in formation rate raised to the power of response ($f_O \approx f_I^R$). As the responses $R_{\mathrm{NUC,POW}}$ are close to zero, significant changes in cluster formation rates are required to substantially affect CCN concentrations. Therefore, in the presence of primary particle emissions, cluster formation is suppressed to levels where its impact on CCN formation is not showing its full potential, which would be seen in cleaner air with low background concentration and condensation sink. While nucleation still remains significant in creating CCN, particularly during daytime and higher supersaturation size classes, primary emissions strongly affect the CCN concentrations under current conditions. The ZeroPNE simulation suggests that without primary aerosol emissions, more than half of [$\mathrm{CCN}_{0.5\%}$] and higher supersaturation classes would remain, whereas the lowest supersaturation CCN would drop significantly. However, cloud processes and related aqueous-phase inorganic chemistry could impact these conclusions (e.g. Xavier et al., 2022). Furthermore, the ZeroPNE simulation was not a true pre-industrial scenario, as other anthropogenic emissions, including SO_2, were as in BASE.

A notable finding is that increased cluster formation often lowers concentrations of the largest CCN. This behaviour has already been found in other modelling studies (Roldin et al., 2019; Patoulias et al., 2024), and would affect cloud droplet numbers in stratiform clouds with weak updrafts. The only process in the model responsible for this is the depletion of low-volatility vapours which would otherwise accumulate on Aitken mode particles. During the time of largest negative effect

https://doi.org/10.5194/egusphere-2025-39
Preprint. Discussion started: 7 January 2025
© Author(s) 2025. CC BY 4.0 License.

[$CCN_{0.1\%}$] were very low, indicating that the PNE size distribution at the time was low on the accumulation mode particles which would otherwise dominate the condensation sink, and therefore the nucleation mode from NPF and primary emissions would be comparable sinks of vapours.

The sources of airmasses during high SOA mass at the station (usually between southerly to easterly origins at SMEAR II) do not in general coincide with those that are connected to strong new particle formation events (northerly or north-westerly origins), while strong BVOC emissions along the trajectory noticeably coincide with elevated PNE. Consistent with the southerly origins of BVOC, modelled OA mass correlates with mean temperature along the trajectory, aligning with prior studies based on local observations and trajectory analysis (e.g. Paasonen et al., 2013; Yli-Juuti et al., 2021). The strong [CCN] response to PNE and weak response to cluster formation rates highlight the difficulty the nanometre-sized particles, forming in NPF, face when growing to CCN sizes, while emitted particles are already at, or close to, activation size, and furthermore can grow from a larger pool of low volatility vapours.

On average, SOSAA overestimated the particle concentrations in the 1–30 nm diameter range, but still underestimated the Aitken mode. Paasonen et al. (2016) estimated that the applied PNE in nucleation mode are clearly underestimated, which has been confirmed by observations in Beijing (Kontkanen et al., 2020). Overestimating the concentrations while very likely underestimating the emissions in this size range would suggest that the growth of the newly formed particles is not sufficiently efficient in the model. While the overshooting concentrations in nucleation mode can be attributed to more frequent new particle formation in SOSAA compared to what is observed at SMEAR II, the missing Aitken mode particles would result from low survivability (high coagulation sink) and insufficient growth of the particles. When comparing the modelled and measured sulfuric acid and HOM concentrations, the model does not suffer from a considerable lack of low volatility vapours. Still, SOSAA-FP chemistry module in this work did not have autoxidation scheme from aromatics, meaning that some low volatility vapours are still missing from the model. The enhancing effect of AVOC emissions on SOA production is well known generally (Riva et al., 2019) and that aromatic compounds (e.g. benzenes, polyaromatics and cycloalkanes) common in anthropogenic emissions markedly enhance production yields of highly oxidized molecules in the atmosphere through auto-oxidation reactions, and thus increase SOA mass (Rissanen, 2021). Furthermore, it is possible that the condensational growth alone is not able to reproduce the observed size distributions, at least with these saturation vapour pressures, but e.g. surface reactions and inorganic chemistry could play a significant role in enhancing SOA yields though mechanisms so far unaccounted for in the SOSAA model. Given how sluggishly the nucleation mode particles grow to CCN size, we should also not rule out that the gap in 30–300 nm modelled and observed number concentrations could simply come from underestimations in the particle emission dataset, further underlining the importance of proper estimations of primary number emissions in the CCN processes.

While this study did not focus on the meteorology, much of the dynamics and variation is strongly influenced by the meteorology. The airmass trajectories themselves are the result of atmospheric circulation, driven by the distribution of the solar energy. The environmental conditions and geographic locations along the trajectories set strong boundaries to which processes

https://doi.org/10.5194/egusphere-2025-39
Preprint. Discussion started: 7 January 2025
© Author(s) 2025. CC BY 4.0 License.

will dominate CCN formation. These constraints should be kept in mind when interpreting local observations and the processes that led to them.

The key part of CCN formation from NPF in boreal forest environment is the efficient growth of the nucleation mode particles. During the development of this model and early experiments, it became evident that just increasing BVOC emissions did not solve this conundrum, as the majority of low volatility vapours were accumulating on the larger particles, leading to overestimation compared to both aerosol mass and [HOM] measurements at SMEAR II, without significant shift of the nucleation mode towards Aitken and CCN sizes. It seems that the vapour pressure based approach (which for extremely low volatility vapours and H_2SO_4 compounds in practice means condensation at kinetic limit) to gas-particle partitioning is not enough to reproduce the straightforward pathway of cluster formation to CCN in a detailed model such as SOSAA. Whether there is a process that either increases the survivability of the nucleation mode particles beyond what the Brownian coagulation model assumes, or if for example heterogenous chemistry on the nucleation mode particles increases their growth rates well beyond that calculated by the Kelvin theory, can be speculated, and is something that should be investigated in more depth. Box models that utilize similar aerosol chemistry and physics have been evaluated in chamber experiments to the extent that doubting the modelling of coagulation seems unnecessary, and on the other hand the recent advances in heterogeneous chemistry of particles in the atmosphere give hope that these processes can be included in future atmospheric models. Meanwhile, these modelling results highlight the extremely dynamic and convoluted relation between atmospheric aerosol formation and primary emissions. While the more direct pathway from NPF to CCN could still be the main driver in remote locations, in the geographic region relevant to this study (Northern Europe), anthropogenic influence is strong, despite the rural nature of the SMEAR II station itself. The results show that even with much improved air quality and emission control in the last decades, human influence on the atmospheric fine particles is substantial.

Acknowledgements and financial support

The authors wish to thank the Finnish CSC – IT Center for Science Ltd. for providing invaluable HPC resources for this study. PC gratefully acknowledges the University of Edinburgh and University of Helsinki Partnership Programme on Forests. We acknowledge the FLEXPART development team (FlexTeam, University of Vienna; flex team.univie.ac.at).

Financial support

Financial support was provided through the Research Council of Finland (projects 360114, ACCC 337549) and Horizon Europe project FOCI (101056783). Additionally, this project was funded by internal resources at the University of Helsinki's Lahti University Campus.

https://doi.org/10.5194/egusphere-2025-39
Preprint. Discussion started: 7 January 2025
© Author(s) 2025. CC BY 4.0 License.

Code/Data availability

The processed model data used for figures is available at https://doi.org/10.5281/zenodo.14602389 (Clusius, 2025). SOSAA-FP code, and full model input and output is available at request from the corresponding author.

Author contribution

MB and PIP outlined the study. PC, MBa, CX, PZ, JT, PP performed the model development and data preprocessing, PC conducted the simulations and evaluations, analyzed the simulation results, wrote the original paper and plotted all figures, under supervision of PP, MB and PIP. MÄ, FG processed and provided ACSM data. All authors contributed to the paper preparation, discussion, and writing.

Competing interests

The authors declare that they have no conflict of interest.

References

Aalto, P., Hämeri, K., Becker, E., Weber, R., Salm, J., Mäkelä, Jyrki M.., Hoell, C., O'Dowd, Colin D.., Karlsson, H., Hansson, H.-C., Väkevä, M., Koponen, Ismo K.., Buzorius, G. and Kulmala, M.: Physical characterization of aerosol particles during nucleation events, Tellus. Series B: Chemical and Physical Meteorology, 53, 344-358, 10.1034/j.1600-0889.2001.530403.x, 2001.

Allan, J. D., Alfarra, M. R., Bower, K. N., Coe, H., Jayne, J. T., Worsnop, D. R., Aalto, P. P., Kulmala, M., Hyötyläinen, T., Cavalli, F. and Laaksonen, A.: Size and composition measurements of background aerosol and new particle growth in a Finnish forest during QUEST 2 using an Aerodyne Aerosol Mass Spectrometer, Atmos. Chem. Phys., 6, 315-327, 10.5194/acp-6-315-2006, 2006.

Almeida, J., Schobesberger, S., Kürten, A., Ortega, I. K., Kupiainen-Määttä, O., Praplan, A. P., Adamov, A., Amorim, A., Bianchi, F., Breitenlechner, M., David, A., Dommen, J., Donahue, N. M., Downard, A., Dunne, E., Duplissy, J., Ehrhart, S., Flagan, R. C., Franchin, A., Guida, R., Hakala, J., Hansel, A., Heinritzi, M., Henschel, H., Jokinen, T., Junninen, H., Kajos, M., Kangasluoma, J., Keskinen, H., Kupc, A., Kurtén, T., Kvashin, A. N., Laaksonen, A., Lehtipalo, K., Leiminger, M., Leppä, J., Loukonen, V., Makhmutov, V., Mathot, S., McGrath, M. J., Nieminen, T., Olenius, T., Onnela, A., Petäjä, T., Riccobono, F., Riipinen, I., Rissanen, M., Rondo, L., Ruuskanen, T., Santos, F. D., Sarnela, N., Schallhart, S., Schnitzhofer, R., Seinfeld, J. H., Simon, M., Sipilä, M., Stozhkov, Y., Stratmann, F., Tomé, A., Tröstl, J., Tsagkogeorgas, G., Vaattovaara, P., Viisanen, Y., Virtanen, A., Vrtala, A., Wagner, P. E., Weingartner, E., Wex, H., Williamson, C., Wimmer, D., Ye, P., Yli-Juuti, T., Carslaw, K. S., Kulmala, M., Curtius,

https://doi.org/10.5194/egusphere-2025-39
Preprint. Discussion started: 7 January 2025
© Author(s) 2025. CC BY 4.0 License.

J., Baltensperger, U., Worsnop, D. R., Vehkamäki, H. and Kirkby, J.: Molecular understanding of sulphuric acid–amine particle nucleation in the atmosphere, Nature, 502, 359–363, https://doi.org/10.1038/nature12663, 2013.

Amann, M., Bertok, I., Borken-Kleefeld, J., Cofala, J., Heyes, C., Höglund-Isaksson, L., Klimont, Z., Nguyen, B., Posch, M., Rafaj, P., Sandler, R., Schöpp, W., Wagner, F. and Winiwarter, W.: Cost-effective control of air quality and greenhouse gases in Europe: Modeling and policy applications, Environmental Modelling & Software, 26, 1489-1501, 10.1016/j.envsoft.2011.07.012, 2011.

Behera, S. N., Sharma, M., Aneja, V. P. and Balasubramanian, R.: Ammonia in the atmosphere: a review on emission sources, atmospheric chemistry and deposition on terrestrial bodies, Environ. Sci. Pollut. Res., 20, 8092–8131, https://doi.org/10.1007/s11356-013-2051-9, 2013.

Besel, V., Kubečka, J., Kurtén, T. and Vehkamäki, H.: Impact of Quantum Chemistry Parameter Choices and Cluster Distribution Model Settings on Modeled Atmospheric Particle Formation Rates, J. Phys. Chem. A, 124, 5931–5943, https://doi.org/10.1021/acs.jpca.0c03984, 2020.

Bianchi, F., Kurtén, T., Riva, M., Mohr, C., Rissanen, M. P., Roldin, P., Berndt, T., Crounse, J. D., Wennberg, P. O., Mentel, T. F., Wildt, J., Junninen, H., Jokinen, T., Kulmala, M., Worsnop, D. R., Thornton, J. A., Donahue, N., Kjaergaard, H. G. and Ehn, M.: Highly Oxygenated Organic Molecules (HOM) from Gas-Phase Autoxidation Involving Peroxy Radicals: A Key Contributor to Atmospheric Aerosol, Chem. Rev., 119, 3472-3509, 10.1021/acs.chemrev.8b00395, 2019.

Blake, R. S., Monks, P. S. and Ellis, A. M.: Proton-Transfer Reaction Mass Spectrometry, Chem. Rev., 109, 861-896, 10.1021/cr800364q, 2009.

Boy, M., Zhou, P., Kurtén, T., Chen, D., Xavier, C., Clusius, P., Roldin, P., Baykara, M., Pichelstorfer, L., Foreback, B., Bäck, J., Petäjä, T., Makkonen, R., Kerminen, V.-M., Pihlatie, M., Aalto, J. and Kulmala, M.: Positive feedback mechanism between biogenic volatile organic compounds and the methane lifetime in future climates, npj Climate and Atmospheric Science, 5, 10.1038/s41612-022-00292-0, 2022.

Chamba, G., Rissanen, M., Barthelmeß, T., Saiz-Lopez, A., Rose, C., Iyer, S., Saint-Macary, A., Rocco, M., Safi, K., Deppeler, S., Barr, N., Harvey, M., Engel, A., Dunne, E., Law, C. S. and Sellegri, K.: Evidence of nitrate-based nighttime atmospheric nucleation driven by marine microorganisms in the South Pacific, Proc. Natl. Acad. Sci., 120, 10.1073/pnas.2308696120, 2023.

Chen, D., Xavier, C., Clusius, P., Nieminen, T., Roldin, P., Qi, X., Pichelstorfer, L., Kulmala, M., Rantala, P., Aalto, J., Sarnela, N., Kolari, P., Keronen, P., Rissanen, M. P., Taipale, D., Foreback, B., Baykara, M., Zhou, P. and Boy, M.: A modelling study of OH, NO3 and H2SO4 in 2007–2018 at SMEAR II, Finland: analysis of long-term trends, Environmental Science: Atmospheres, 1, 449-472, 10.1039/d1ea00020a, 2021.

Clusius, P.: SOSAA-FP postprocessed aerosol data from base and sensitivity simulations, 2025.

Clusius, P., Xavier, C., Pichelstorfer, L., Zhou, P., Olenius, T., Roldin, P. and Boy, M.: Atmospherically Relevant Chemistry and Aerosol box model – ARCA box (version 1.2), Geosci. Model Dev., 15, 7257-7286, 10.5194/gmd-15-7257-2022, 2022.

Crippa, M., Guizzardi, D., Muntean, M., Schaaf, E., Dentener, F., van Aardenne, J. A., Monni, S., Doering, U., Olivier, J. G. J., Pagliari, V. and Janssens-Maenhout, G.: Gridded emissions of air pollutants for the period 1970–2012 within EDGAR v4.3.2, Earth Syst. Sci. Data, 10, 1987-2013, 10.5194/essd-10-1987-2018, 2018.

https://doi.org/10.5194/egusphere-2025-39
Preprint. Discussion started: 7 January 2025
© Author(s) 2025. CC BY 4.0 License.

Dada, L., Paasonen, P., Nieminen, T., Mazon, S. B., Kontkanen, J., Peräkylä, O., Lehtipalo, K., Hussein, T., Petäjä, T., Kerminen, V.-M., Bäck, J. and Kulmala, M.: Long-term analysis of clear-sky new particle formation events and nonevents in Hyytiälä, Atmos. Chem. Phys., 17, 6227–6241, https://doi.org/10.5194/acp-17-6227-2017, 2017.

Dada, L., Stolzenburg, D., Simon, M., Fischer, L., Heinritzi, M., Wang, M., Xiao, M., Vogel, A. L., Ahonen, L., Amorim, A., Baalbaki, R., Baccarini, A., Baltensperger, U., Bianchi, F., Daellenbach, K. R., DeVivo, J., Dias, A., Dommen, J., Duplissy, J., Finkenzeller, H., Hansel, A., He, X.-C., Hofbauer, V., Hoyle, C. R., Kangasluoma, J., Kim, C., Kürten, A., Kvashnin, A., Mauldin, R., Makhmutov, V., Marten, R., Mentler, B., Nie, W., Petäjä, T., Quéléver, L. L. J., Saathoff, H., Tauber, C., Tome, A., Molteni, U., Volkamer, R., Wagner, R., Wagner, A. C., Wimmer, D., Winkler, P. M., Yan, C., Zha, Q., Rissanen, M., Gordon, H., Curtius, J., Worsnop, D. R., Lehtipalo, K., Donahue, N. M., Kirkby, J., El Haddad, I. and Kulmala, M.: Role of sesquiterpenes in biogenic new particle formation, Sci. Adv., 9, 10.1126/sciadv.adi5297, 2023.

Donahue, N. M., Epstein, S. A., Pandis, S. N. and Robinson, A. L.: A two-dimensional volatility basis set: 1. organic-aerosol mixing thermodynamics, Atmos. Chem. Phys., 11, 3303-3318, 10.5194/acp-11-3303-2011, 2011.

Dunne, E. M., Gordon, H., Kürten, A., Almeida, J., Duplissy, J., Williamson, C., Ortega, I. K., Pringle, K. J., Adamov, A., Baltensperger, U., Barmet, P., Benduhn, F., Bianchi, F., Breitenlechner, M., Clarke, A., Curtius, J., Dommen, J., Donahue, N. M., Ehrhart, S., Flagan, R. C., Franchin, A., Guida, R., Hakala, J., Hansel, A., Heinritzi, M., Jokinen, T., Kangasluoma, J., Kirkby, J., Kulmala, M., Kupc, A., Lawler, M. J., Lehtipalo, K., Makhmutov, V., Mann, G., Mathot, S., Merikanto, J., Miettinen, P., Nenes, A., Onnela, A., Rap, A., Reddington, C. L. S., Riccobono, F., Richards, N. A. D., Rissanen, M. P., Rondo, L., Sarnela, N., Schobesberger, S., Sengupta, K., Simon, M., Sipilä, M., Smith, J. N., Stozkhov, Y., Tomé, A., Tröstl, J., Wagner, P. E., Wimmer, D., Winkler, P. M., Worsnop, D. R. and Carslaw, K. S.: Global atmospheric particle formation from CERN CLOUD measurements, Science, 354, 1119-1124, 10.1126/science.aaf2649, 2016.

Dusek, U., Frank, G. P., Hildebrandt, L., Curtius, J., Schneider, J., Walter, S., Chand, D., Drewnick, F., Hings, S., Jung, D., Borrmann, S. and Andreae, M. O.: Size Matters More Than Chemistry for Cloud-Nucleating Ability of Aerosol Particles, Science, 312, 1375–1378, https://doi.org/10.1126/science.1125261, 2006.

Ehn, M., Thornton, J. A., Kleist, E., Sipilä, M., Junninen, H., Pullinen, I., Springer, M., Rubach, F., Tillmann, R., Lee, B., Lopez-Hilfiker, F., Andres, S., Acir, I.-H., Rissanen, M., Jokinen, T., Schobesberger, S., Kangasluoma, J., Kontkanen, J., Nieminen, T., Kurtén, T., Nielsen, L. B., Jørgensen, S., Kjaergaard, H. G., Canagaratna, M., Maso, M. D., Berndt, T., Petäjä, T., Wahner, A., Kerminen, V.-M., Kulmala, M., Worsnop, D. R., Wildt, J. and Mentel, T. F.: A large source of low-volatility secondary organic aerosol, Nature, 506, 476–479, https://doi.org/10.1038/nature13032, 2014.

Elm, J., Kubečka, J., Besel, V., Jääskeläinen, M. J., Halonen, R., Kurtén, T. and Vehkamäki, H.: Modeling the formation and growth of atmospheric molecular clusters: A review, J. Aerosol Sci., 149, 105621, 10.1016/j.jaerosci.2020.105621, 2020.

EPA: Guidance on the Use of Models and Other Analyses for Demonstrating Attainment of Air Quality Goals for Ozone, PM2.5, and Regional Haze, Vol EPA-454/B-07e002, 2007.

Garmash, O., Rissanen, M. P., Pullinen, I., Schmitt, S., Kausiala, O., Tillmann, R., Zhao, D., Percival, C., Bannan, T. J., Priestley, M., Hallquist, Å. M., Kleist, E., Kiendler-Scharr, A., Hallquist, M., Berndt, T., McFiggans, G., Wildt, J., Mentel, T. F. and Ehn, M.: Multi-generation OH oxidation as a source for highly oxygenated organic molecules from aromatics, Atmos. Chem. Phys., 20, 515-537, 10.5194/acp-20-515-2020, 2020.

https://doi.org/10.5194/egusphere-2025-39
Preprint. Discussion started: 7 January 2025
© Author(s) 2025. CC BY 4.0 License.

Denier van der Gon, H., Visschedijk, A., Johansson, C., Larsson, E. H., Harrison, R. M. and Beddows, D.: Size-resolved Pan European Anthropogenic Particle Number Inventory, EU-CAARI Deliverable D141, 2009.

Gordon, H., Kirkby, J., Baltensperger, U., Bianchi, F., Breitenlechner, M., Curtius, J., Dias, A., Dommen, J., Donahue, N. M., Dunne, E. M., Duplissy, J., Ehrhart, S., Flagan, R. C., Frege, C., Fuchs, C., Hansel, A., Hoyle, C. R., Kulmala, M., Kürten, A., Lehtipalo, K., Makhmutov, V., Molteni, U., Rissanen, M. P., Stozkhov, Y., Tröstl, J., Tsagkogeorgas, G., Wagner, R., Williamson, C., Wimmer, D., Winkler, P. M., Yan, C. and Carslaw, K. S.: Causes and importance of new particle formation in the present-day and preindustrial atmospheres, Journal of Geophysical Research: Atmospheres, 122, 8739-8760, 10.1002/2017jd026844, 2017.

Granier, C., Darras, S., Denier van der Gon, H., Doubalova, J., Elguindi, N., Galle, B., Gauss, M., Guevara, M., Jalkanen, J.-P., Kuenen, J., Liousse, C., Quack, B., Simpson, D. and Sindelarova, K.: The Copernicus Atmosphere Monitoring Service global and regional emissions (April 2019 version), 2019.

Guenther, A. B., Jiang, X., Heald, C. L., Sakulyanontvittaya, T., Duhl, T., Emmons, L. K. and Wang, X.: The Model of Emissions of Gases and Aerosols from Nature version 2.1 (MEGAN2.1): an extended and updated framework for modeling biogenic emissions, Geosci. Model Dev., 5, 1471-1492, 10.5194/gmd-5-1471-2012, 2012.

Guevara, M., Jorba, O., Tena, C., Denier van der Gon, H., Kuenen, J., Elguindi, N., Darras, S., Granier, C. and Pérez García-Pando, C.: Copernicus Atmosphere Monitoring Service TEMPOral profiles (CAMS-TEMPO): global and European emission temporal profile maps for atmospheric chemistry modelling, Earth Syst. Sci. Data, 13, 367-404, 10.5194/essd-13-367-2021, 2021.

Haataja, J. & Vesala, T.: Smear - II: station for measuring forest ecosystem - atmosphere relations, in: , edited by: J. Haataja & T. Vesala, Helsingin yliopiston metsäekologian laitos, Helsinki, 1997.

Hakala, S., Vakkari, V., Lihavainen, H., Hyvärinen, A.-P., Neitola, K., Kontkanen, J., Kerminen, V.-M., Kulmala, M., Petäjä, T., Hussein, T., Khoder, M. I., Alghamdi, M. A. and Paasonen, P.: Explaining apparent particle shrinkage related to new particle formation events in western Saudi Arabia does not require evaporation, Atmos. Chem. Phys., 23, 9287-9321, 10.5194/acp-23-9287-2023, 2023.

Hari, P. and Kulmala, M.: Station for Measuring Ecosystem-Atmosphere Relations (SMEAR II), Boreal Environ. Res., 10, 315-322, 2005.

Heikkinen, L., Äijälä, M., Riva, M., Luoma, K., Dällenbach, K., Aalto, J., Aalto, P., Aliaga, D., Aurela, M., Keskinen, H., Makkonen, U., Rantala, P., Kulmala, M., Petäjä, T., Worsnop, D. and Ehn, M.: Long-term sub-micrometer aerosol chemical composition in the boreal forest: inter- and intra-annual variability, Atmos. Chem. Phys., 20, 3151-3180, 10.5194/acp-20-3151-2020, 2020.

Hersbach, H., Bell, B., Berrisford, P., Biavati, G., Horányi, A., Sabater, J. M., Nicolas, J., Peubey, C., Radu, R., Rozum, I., Schepers, D., Simmons, A., Soci, C., Dee, D. and Thépaut, J.-N.: ERA5 hourly data on single levels from 1940 to present, 2018.

Hersbach, H., Bell, B., Berrisford, P., Hirahara, S., Horányi, A., Muñoz-Sabater, J., Nicolas, J., Peubey, C., Radu, R., Schepers, D., Simmons, A., Soci, C., Abdalla, S., Abellan, X., Balsamo, G., Bechtold, P., Biavati, G., Bidlot, J., Bonavita, M., De Chiara, G., Dahlgren, P., Dee, D., Diamantakis, M., Dragani, R., Flemming, J., Forbes, R., Fuentes, M., Geer, A., Haimberger, L., Healy, S., Hogan, R. J., Hólm, E., Janisková, M., Keeley, S., Laloyaux, P., Lopez, P., Lupu, C., Radnoti, G., de Rosnay, P., Rozum, I., Vamborg, F., Villaume, S. and Thépaut, J.: The ERA5 global reanalysis, Q. J. R. Meteorolog. Soc., 146, 1999-2049, 10.1002/qj.3803, 2020.

https://doi.org/10.5194/egusphere-2025-39
Preprint. Discussion started: 7 January 2025
© Author(s) 2025. CC BY 4.0 License.

Hirsikko, A., Nieminen, T., Gagné, S., Lehtipalo, K., Manninen, H. E., Ehn, M., Hõrrak, U., Kerminen, V.-M., Laakso, L., McMurry, P. H., Mirme, A., Mirme, S., Petäjä, T., Tammet, H., Vakkari, V., Vana, M. and Kulmala, M.: Atmospheric ions and nucleation: a review of observations, Atmos. Chem. Phys., 11, 767-798, 10.5194/acp-11-767-2011, 2011.

Hoesly, R. M., Smith, S. J., Feng, L., Klimont, Z., Janssens-Maenhout, G., Pitkanen, T., Seibert, J. J., Vu, L., Andres, R. J., Bolt, R. M., Bond, T. C., Dawidowski, L., Kholod, N., Kurokawa, J.-i., Li, M., Liu, L., Lu, Z., Moura, M. C. P., O'Rourke, P. R. and Zhang, Q.: Historical (1750–2014) anthropogenic emissions of reactive gases and aerosols from the Community Emissions Data System (CEDS), Geosci. Model Dev., 11, 369-408, 10.5194/gmd-11-369-2018, 2018.

Huang, G., Brook, R., Crippa, M., Janssens-Maenhout, G., Schieberle, C., Dore, C., Guizzardi, D., Muntean, M., Schaaf, E. and Friedrich, R.: Speciation of anthropogenic emissions of non-methane volatile organic compounds: a global gridded data set for 1970–2012, Atmos. Chem. Phys., 17, 7683-7701, 10.5194/acp-17-7683-2017, 2017.

Ilvesniemi, H., Levula, J., Ojansuu, R., Kolari, P., Kulmala, L., Pumpanen, J., Launiainen, S., Vesala, T. and Nikinmaa, E.: Long-term measurements of the carbon balance of a boreal Scots pine dominated forest ecosystem, Boreal Environ. Res., 14, 731-753, 2009.

Jacobson, M. Z.: Development and application of a new air pollution modeling system—II. Aerosol module structure and design, Atmos. Environ., 31, 131–144, https://doi.org/10.1016/1352-2310(96)00202-6, 1997.

Jacobson, M. Z.: Analysis of aerosol interactions with numerical techniques for solving coagulation, nucleation, condensation, dissolution, and reversible chemistry among multiple size distributions, J. Geophys. Res., 107, AAC 2-1-AAC 2-23, https://doi.org/10.1029/2001jd002044, 2002.

Jenkin, M. E., Saunders, S. M. and Pilling, M. J.: The tropospheric degradation of volatile organic compounds: a protocol for mechanism development, Atmos. Environ., 31, 81–104, https://doi.org/10.1016/s1352-2310(96)00105-7, 1997.

Jenkin, M. E., Young, J. C. and Rickard, A. R.: The MCM v3.3.1 degradation scheme for isoprene, Atmos. Chem. Phys., 15, 11433–11459, https://doi.org/10.5194/acp-15-11433-2015, 2015.

Jeričević, A., Kraljević, L., Grisogono, B., Fagerli, H. and Večenaj, Ž.: Parameterization of vertical diffusion and the atmospheric boundary layer height determination in the EMEP model, Atmos. Chem. Phys., 10, 341-364, 10.5194/acp-10-341-2010, 2010.

Junninen, H., Lauri, A., Keronen, P., Aalto, P., Hiltunen, V., Hari, P. and Kulmala, M.: Smart-SMEAR: on-line data exploration and visualization tool for SMEAR stations, Boreal Environ. Res., 14, 447-457, 2009.

Kerminen, V.-M., Paramonov, M., Anttila, T., Riipinen, I., Fountoukis, C., Korhonen, H., Asmi, E., Laakso, L., Lihavainen, H., Swietlicki, E., Svenningsson, B., Asmi, A., Pandis, S. N., Kulmala, M. and Petäjä, T.: Cloud condensation nuclei production associated with atmospheric nucleation: a synthesis based on existing literature and new results, Atmos. Chem. Phys., 12, 12037–12059, https://doi.org/10.5194/acp-12-12037-2012, 2012.

Keronen, P. (2017). Flux and concentration measurements of carbon dioxide and ozone in a forested environment [Doctor Dissertation]. Finland: University of Helsinki.

Kirkby, J., Curtius, J., Almeida, J., Dunne, E., Duplissy, J., Ehrhart, S., Franchin, A., Gagné, S., Ickes, L., Kürten, A., Kupc, A., Metzger, A., Riccobono, F., Rondo, L., Schobesberger, S., Tsagkogeorgas, G., Wimmer, D., Amorim, A.,

https://doi.org/10.5194/egusphere-2025-39
Preprint. Discussion started: 7 January 2025
© Author(s) 2025. CC BY 4.0 License.

Bianchi, F., Breitenlechner, M., David, A., Dommen, J., Downard, A., Ehn, M., Flagan, R. C., Haider, S., Hansel, A., Hauser, D., Jud, W., Junninen, H., Kreissl, F., Kvashin, A., Laaksonen, A., Lehtipalo, K., Lima, J., Lovejoy, E. R., Makhmutov, V., Mathot, S., Mikkilä, J., Minginette, P., Mogo, S., Nieminen, T., Onnela, A., Pereira, P., Petäjä, T., Schnitzhofer, R., Seinfeld, J. H., Sipilä, M., Stozhkov, Y., Stratmann, F., Tomé, A., Vanhanen, J., Viisanen, Y., Vrtala, A., Wagner, P. E., Walther, H., Weingartner, E., Wex, H., Winkler, P. M., Carslaw, K. S., Worsnop, D. R., Baltensperger, U. and Kulmala, M.: Role of sulphuric acid, ammonia and galactic cosmic rays in atmospheric aerosol nucleation, Nature, 476, 429-433, 10.1038/nature10343, 2011.

Klimont, Z., Kupiainen, K., Heyes, C., Purohit, P., Cofala, J., Rafaj, P., Borken-Kleefeld, J. and Schöpp, W.: Global anthropogenic emissions of particulate matter including black carbon, Atmos. Chem. Phys., 17, 8681-8723, 10.5194/acp-17-8681-2017, 2017.

Kolari, P., Aalto, J., Levula, J., Kulmala, L., Ilvesniemi, H. and Pumpanen, J.: Hyytiälä SMEAR II site characteristics, 2022.

Kontkanen, J., Deng, C., Fu, Y., Dada, L., Zhou, Y., Cai, J., Daellenbach, K. R., Hakala, S., Kokkonen, T. V., Lin, Z., Liu, Y., Wang, Y., Yan, C., Petäjä, T., Jiang, J., Kulmala, M. and Paasonen, P.: Size-resolved particle number emissions in Beijing determined from measured particle size distributions, Atmos. Chem. Phys., 20, 11329-11348, 10.5194/acp-20-11329-2020, 2020.

Kulmala, M., Asmi, A., Lappalainen, H. K., Baltensperger, U., Brenguier, J.-L., Facchini, M. C., Hansson, H.-C., Hov, Ø., O'Dowd, C. D., Pöschl, U., Wiedensohler, A., Boers, R., Boucher, O., de Leeuw, G., Denier van der Gon, H. A. C., Feichter, J., Krejci, R., Laj, P., Lihavainen, H., Lohmann, U., McFiggans, G., Mentel, T., Pilinis, C., Riipinen, I., Schulz, M., Stohl, A., Swietlicki, E., Vignati, E., Alves, C., Amann, M., Ammann, M., Arabas, S., Artaxo, P., Baars, H., Beddows, D. C. S., Bergström, R., Beukes, J. P., Bilde, M., Burkhart, J. F., Canonaco, F., Clegg, S. L., Coe, H., Crumeyrolle, S., D'Anna, B., Decesari, S., Gilardoni, S., Fischer, M., Fjaeraa, A. M., Fountoukis, C., George, C., Gomes, L., Halloran, P., Hamburger, T., Harrison, R. M., Herrmann, H., Hoffmann, T., Hoose, C., Hu, M., Hyvärinen, A., Hõrrak, U., Iinuma, Y., Iversen, T., Josipovic, M., Kanakidou, M., Kiendler-Scharr, A., Kirkevåg, A., Kiss, G., Klimont, Z., Kolmonen, P., Komppula, M., Kristjánsson, J.-E., Laakso, L., Laaksonen, A., Labonnote, L., Lanz, V. A., Lehtinen, K. E. J., Rizzo, L. V., Makkonen, R., Manninen, H. E., McMeeking, G., Merikanto, J., Minikin, A., Mirme, S., Morgan, W. T., Nemitz, E., O'Donnell, D., Panwar, T. S., Pawlowska, H., Petzold, A., Pienaar, J. J., Pio, C., Plass-Duelmer, C., Prévôt, A. S. H., Pryor, S., Reddington, C. L., Roberts, G., Rosenfeld, D., Schwarz, J., Seland, Ø., Sellegri, K., Shen, X. J., Shiraiwa, M., Siebert, H., Sierau, B., Simpson, D., Sun, J. Y., Topping, D., Tunved, P., Vaattovaara, P., Vakkari, V., Veefkind, J. P., Visschedijk, A., Vuollekoski, H., Vuolo, R., Wehner, B., Wildt, J., Woodward, S., Worsnop, D. R., van Zadelhoff, G.-J., Zardini, A. A., Zhang, K., van Zyl, P. G., Kerminen, V.-M., S Carslaw, K. and Pandis, S. N.: General overview: European Integrated project on Aerosol Cloud Climate and Air Quality interactions (EUCAARI) – integrating aerosol research from nano to global scales, Atmos. Chem. Phys., 11, 13061-13143, 10.5194/acp-11-13061-2011, 2011.

Kulmala, M., Asmi, A., Lappalainen, H. K., Carslaw, K. S., Pöschl, U., Baltensperger, U., Hov, Ø., Brenquier, J.-L., Pandis, S. N., Facchini, M. C., Hansson, H.-C., Wiedensohler, A. and O'Dowd, C. D.: Introduction: European Integrated Project on Aerosol Cloud Climate and Air Quality interactions (EUCAARI) – integrating aerosol research from nano to global scales, Atmos. Chem. Phys., 9, 2825-2841, 10.5194/acp-9-2825-2009, 2009.

Kulmala, M., Rannik, U., Pirjola, L., Dal Maso, M., Karimäki, J., Asmi, A., Jäppinen, A., Karhu, V., Korhonen, H., Malvikko, S.-P., Raittila, J., Suni, T., Yli-Koivisto, S. and Vesala, T.: Characterization of atmospheric trace gas and

https://doi.org/10.5194/egusphere-2025-39
Preprint. Discussion started: 7 January 2025
© Author(s) 2025. CC BY 4.0 License.

aerosol concentrations at forest sites in southern and northern Finland using back trajectories, Boreal environment research : an international interdisciplinary journal, 315-336, 2000.

Kürten, A., Bianchi, F., Almeida, J., Kupiainen-Määttä, O., Dunne, E. M., Duplissy, J., Williamson, C., Barmet, P., Breitenlechner, M., Dommen, J., Donahue, N. M., Flagan, R. C., Franchin, A., Gordon, H., Hakala, J., Hansel, A., Heinritzi, M., Ickes, L., Jokinen, T., Kangasluoma, J., Kim, J., Kirkby, J., Kupc, A., Lehtipalo, K., Leiminger, M., Makhmutov, V., Onnela, A., Ortega, I. K., Petäjä, T., Praplan, A. P., Riccobono, F., Rissanen, M. P., Rondo, L., Schnitzhofer, R., Schobesberger, S., Smith, J. N., Steiner, G., Stozhkov, Y., Tomé, A., Tröstl, J., Tsagkogeorgas, G., Wagner, P. E., Wimmer, D., Ye, P., Baltensperger, U., Carslaw, K., Kulmala, M. and Curtius, J.: Experimental particle formation rates spanning tropospheric sulfuric acid and ammonia abundances, ion production rates, and temperatures, Journal of Geophysical Research: Atmospheres, 121, https://doi.org/10.1002/2015jd023908, 2016.

Li, H., Canagaratna, M. R., Riva, M., Rantala, P., Zhang, Y., Thomas, S., Heikkinen, L., Flaud, P.-M., Villenave, E., Perraudin, E., Worsnop, D., Kulmala, M., Ehn, M. and Bianchi, F.: Atmospheric organic vapors in two European pine forests measured by a Vocus PTR-TOF: insights into monoterpene and sesquiterpene oxidation processes, Atmos. Chem. Phys., 21, 4123-4147, 10.5194/acp-21-4123-2021, 2021.

Lin, H., Long, M. S., Sander, R., Sandu, A., Yantosca, R. M., Estrada, L. A., Shen, L. and Jacob, D. J.: An Adaptive Auto-Reduction Solver for Speeding Up Integration of Chemical Kinetics in Atmospheric Chemistry Models: Implementation and Evaluation in the Kinetic Pre-Processor (KPP) Version 3.0.0, J. Adv. Model. Earth Syst., 15, 10.1029/2022ms003293, 2023.

Lindinger, W. and Jordan, A.: Proton-transfer-reaction mass spectrometry (PTR–MS): on-line monitoring of volatile organic compounds at pptv levels, Chem. Soc. Rev., 27, 347, 10.1039/a827347z, 1998.

Merikanto, J., Spracklen, D. V., Mann, G. W., Pickering, S. J. and Carslaw, K. S.: Impact of nucleation on global CCN, Atmos. Chem. Phys., 9, 8601–8616, https://doi.org/10.5194/acp-9-8601-2009, 2009.

Ng, N. L., Herndon, S. C., Trimborn, A., Canagaratna, M. R., Croteau, P. L., Onasch, T. B., Sueper, D., Worsnop, D. R., Zhang, Q., Sun, Y. L. and Jayne, J. T.: An Aerosol Chemical Speciation Monitor (ACSM) for Routine Monitoring of the Composition and Mass Concentrations of Ambient Aerosol, Aerosol Sci. Technol., 45, 780-794, 10.1080/02786826.2011.560211, 2011.

Olenius, T., Kupiainen-Määttä, O., Ortega, I. K., Kurtén, T. and Vehkamäki, H.: Free energy barrier in the growth of sulfuric acid–ammonia and sulfuric acid–dimethylamine clusters, J. Chem. Phys., 139, 084312, https://doi.org/10.1063/1.4819024, 2013.

Ovadnevaite, J., Manders, A., de Leeuw, G., Ceburnis, D., Monahan, C., Partanen, A.-I., Korhonen, H. and O'Dowd, C. D.: A sea spray aerosol flux parameterization encapsulating wave state, Atmos. Chem. Phys., 14, 1837-1852, 10.5194/acp-14-1837-2014, 2014.

Paasonen, P., Asmi, A., Petäjä, T., Kajos, M. K., Äijälä, M., Junninen, H., Holst, T., Abbatt, J. P. D., Arneth, A., Birmili, W., van der Gon, H. D., Hamed, A., Hoffer, A., Laakso, L., Laaksonen, A., Richard Leaitch, W., Plass-Dülmer, C., Pryor, S. C., Räisänen, P., Swietlicki, E., Wiedensohler, A., Worsnop, D. R., Kerminen, V.-M. and Kulmala, M.: Warming-induced increase in aerosol number concentration likely to moderate climate change, Nat. Geosci., 6, 438-442, 10.1038/ngeo1800, 2013.

Paasonen, P., Kupiainen, K., Klimont, Z., Visschedijk, A., van der Gon, H. A. C. D. and Amann, M.: Continental anthropogenic primary particle number emissions, Atmos. Chem. Phys., 16, 6823-6840, 10.5194/acp-16-6823-2016, 2016.

https://doi.org/10.5194/egusphere-2025-39
Preprint. Discussion started: 7 January 2025
© Author(s) 2025. CC BY 4.0 License.

Paramonov, M., Kerminen, V.-M., Gysel, M., Aalto, P. P., Andreae, M. O., Asmi, E., Baltensperger, U., Bougiatioti, A., Brus, D., Frank, G. P., Good, N., Gunthe, S. S., Hao, L., Irwin, M., Jaatinen, A., Jurányi, Z., King, S. M., Kortelainen, A., Kristensson, A., Lihavainen, H., Kulmala, M., Lohmann, U., Martin, S. T., McFiggans, G., Mihalopoulos, N., Nenes, A., O'Dowd, C. D., Ovadnevaite, J., Petäjä, T., Pöschl, U., Roberts, G. C., Rose, D., Svenningsson, B., Swietlicki, E., Weingartner, E., Whitehead, J., Wiedensohler, A., Wittbom, C. and Sierau, B.: A synthesis of cloud condensation nuclei counter (CCNC) measurements within the EUCAARI network, Atmos. Chem. Phys., 15, 12211-12229, 10.5194/acp-15-12211-2015, 2015.

Patokoski, J., Ruuskanen, T. M., Kajos, M. K., Taipale, R., Rantala, P., Aalto, J., Ryyppö, T., Nieminen, T., Hakola, H. and Rinne, J.: Sources of long-lived atmospheric VOCs at the rural boreal forest site, SMEAR II, Atmos. Chem. Phys., 15, 13413-13432, 10.5194/acp-15-13413-2015, 2015.

Patoulias, D., Florou, K., Pandis, S. N. and Nenes, A.: New Particle Formation Events Can Reduce Cloud Droplets in Boundary Layer Clouds at the Continental Scale, Geophys. Res. Lett., 51, 10.1029/2023gl106182, 2024.

Pennington, M. R., Bzdek, B. R., DePalma, J. W., Smith, J. N., Kortelainen, A.-M., Hildebrandt Ruiz, L., Petäjä, T., Kulmala, M., Worsnop, D. R. and Johnston, M. V.: Identification and quantification of particle growth channels during new particle formation, Atmos. Chem. Phys., 13, 10215-10225, 10.5194/acp-13-10215-2013, 2013.

Petäjä, T., O'Connor, E. J., Moisseev, D., Sinclair, V. A., Manninen, A. J., Väänänen, R., von Lerber, A., Thornton, J. A., Nicoll, K., Petersen, W., Chandrasekar, V., Smith, J. N., Winkler, P. M., Krüger, O., Hakola, H., Timonen, H., Brus, D., Laurila, T., Asmi, E., Riekkola, M.-L., Mona, L., Massoli, P., Engelmann, R., Komppula, M., Wang, J., Kuang, C., Bäck, J., Virtanen, A., Levula, J., Ritsche, M. and Hickmon, N.: BAECC: A Field Campaign to Elucidate the Impact of Biogenic Aerosols on Clouds and Climate, Bull. Am. Meteorol. Soc., 97, 1909-1928, 10.1175/bams-d-14-00199.1, 2016.

Petäjä, T., Tabakova, K., Manninen, A., Ezhova, E., O'Connor, E., Moisseev, D., Sinclair, V. A., Backman, J., Levula, J., Luoma, K., Virkkula, A., Paramonov, M., Räty, M., Äijälä, M., Heikkinen, L., Ehn, M., Sipilä, M., Yli-Juuti, T., Virtanen, A., Ritsche, M., Hickmon, N., Pulik, G., Rosenfeld, D., Worsnop, D. R., Bäck, J., Kulmala, M. and Kerminen, V.-M.: Influence of biogenic emissions from boreal forests on aerosol–cloud interactions, Nat. Geosci., 15, 42-47, 10.1038/s41561-021-00876-0, 2021.

Petters, M. D. and Kreidenweis, S. M.: A single parameter representation of hygroscopic growth and cloud condensation nucleus activity, Atmos. Chem. Phys., 7, 1961-1971, 10.5194/acp-7-1961-2007, 2007.

Pichelstorfer, L., Roldin, P., Rissanen, M., Hyttinen, N., Garmash, O., Xavier, C., Zhou, P., Clusius, P., Foreback, B., Golin Almeida, T., Deng, C., Baykara, M., Kurten, T. and Boy, M.: Towards automated inclusion of autoxidation chemistry in models: from precursors to atmospheric implications, Environmental Science: Atmospheres, 4, 879-896, 10.1039/d4ea00054d, 2024.

Pierce, J. R. and Adams, P. J.: Uncertainty in global CCN concentrations from uncertain aerosol nucleation and primary emission rates, Atmos. Chem. Phys., 9, 1339-1356, 10.5194/acp-9-1339-2009, 2009.

Pierce, J. R., Croft, B., Kodros, J. K., D'Andrea, S. D. and Martin, R. V.: The importance of interstitial particle scavenging by cloud droplets in shaping the remote aerosol size distribution and global aerosol-climate effects, Atmos. Chem. Phys., 15, 6147-6158, 10.5194/acp-15-6147-2015, 2015.

Pierce, J. R., Westervelt, D. M., Atwood, S. A., Barnes, E. A. and Leaitch, W. R.: New-particle formation, growth and climate-relevant particle production in Egbert, Canada: analysis from 1 year of size-distribution observations, Atmos.

https://doi.org/10.5194/egusphere-2025-39
Preprint. Discussion started: 7 January 2025
© Author(s) 2025. CC BY 4.0 License.

Chem. Phys., 14, 8647-8663, 10.5194/acp-14-8647-2014, 2014.

Pisso, I., Sollum, E., Grythe, H., Kristiansen, N. I., Cassiani, M., Eckhardt, S., Arnold, D., Morton, D., Thompson, R. L., Groot Zwaaftink, C. D., Evangeliou, N., Sodemann, H., Haimberger, L., Henne, S., Brunner, D., Burkhart, J. F., Fouilloux, A., Brioude, J., Philipp, A., Seibert, P. and Stohl, A.: The Lagrangian particle dispersion model FLEXPART version 10.4, Geosci. Model Dev., 12, 4955-4997, 10.5194/gmd-12-4955-2019, 2019.

Reddington, C. L., Carslaw, K. S., Spracklen, D. V., Frontoso, M. G., Collins, L., Merikanto, J., Minikin, A., Hamburger, T., Coe, H., Kulmala, M., Aalto, P., Flentje, H., Plass-Dülmer, C., Birmili, W., Wiedensohler, A., Wehner, B., Tuch, T., Sonntag, A., O'Dowd, C. D., Jennings, S. G., Dupuy, R., Baltensperger, U., Weingartner, E., Hansson, H.-C., Tunved, P., Laj, P., Sellegri, K., Boulon, J., Putaud, J.-P., Gruening, C., Swietlicki, E., Roldin, P., Henzing, J. S., Moerman, M., Mihalopoulos, N., Kouvarakis, G., Ždímal, V., Zíková, N., Marinoni, A., Bonasoni, P. and Duchi, R.: Primary versus secondary contributions to particle number concentrations in the European boundary layer, Atmos. Chem. Phys., 11, 12007-12036, 10.5194/acp-11-12007-2011, 2011.

Ren, J., Chen, L., Fan, T., Liu, J., Jiang, S. and Zhang, F.: The NPF Effect on CCN Number Concentrations: A Review and Re-Evaluation of Observations From 35 Sites Worldwide, Geophys. Res. Lett., 48, 10.1029/2021gl095190, 2021.

Renard, J. J., Calidonna, S. E. and Henley, M. V.: Fate of ammonia in the atmosphere - a review for applicability to hazardous releases, J. Hazard. Mater., 108, 29-60, 10.1016/j.jhazmat.2004.01.015, 2004.

Riccobono, F., Schobesberger, S., Scott, C. E., Dommen, J., Ortega, I. K., Rondo, L., Almeida, J., Amorim, A., Bianchi, F., Breitenlechner, M., David, A., Downard, A., Dunne, E. M., Duplissy, J., Ehrhart, S., Flagan, R. C., Franchin, A., Hansel, A., Junninen, H., Kajos, M., Keskinen, H., Kupc, A., Kürten, A., Kvashin, A. N., Laaksonen, A., Lehtipalo, K., Makhmutov, V., Mathot, S., Nieminen, T., Onnela, A., Petäjä, T., Praplan, A. P., Santos, F. D., Schallhart, S., Seinfeld, J. H., Sipilä, M., Spracklen, D. V., Stozhkov, Y., Stratmann, F., Tomé, A., Tsagkogeorgas, G., Vaattovaara, P., Viisanen, Y., Vrtala, A., Wagner, P. E., Weingartner, E., Wex, H., Wimmer, D., Carslaw, K. S., Curtius, J., Donahue, N. M., Kirkby, J., Kulmala, M., Worsnop, D. R. and Baltensperger, U.: Oxidation Products of Biogenic Emissions Contribute to Nucleation of Atmospheric Particles, Science, 344, 717-721, 10.1126/science.1243527, 2014.

Riipinen, I., Pierce, J. R., Yli-Juuti, T., Nieminen, T., Häkkinen, S., Ehn, M., Junninen, H., Lehtipalo, K., Petäjä, T., Slowik, J., Chang, R., Shantz, N. C., Abbatt, J., Leaitch, W. R., Kerminen, V.-M., Worsnop, D. R., Pandis, S. N., Donahue, N. M. and Kulmala, M.: Organic condensation: a vital link connecting aerosol formation to cloud condensation nuclei (CCN) concentrations, Atmos. Chem. Phys., 11, 3865-3878, 10.5194/acp-11-3865-2011, 2011.

Rissanen, M.: Anthropogenic Volatile Organic Compound (AVOC) Autoxidation as a Source of Highly Oxygenated Organic Molecules (HOM), J. Phys. Chem. A, 125, 9027-9039, 10.1021/acs.jpca.1c06465, 2021.

Riuttanen, L., Hulkkonen, M., Dal Maso, M., Junninen, H. and Kulmala, M.: Trajectory analysis of atmospheric transport of fine particles, SO$<sub$>2$</sub$>, NO$<sub$>x$</sub$> and O$<sub$>3$</sub$> to the SMEAR II station in Finland in 1996–2008, Atmos. Chem. Phys., 13, 2153-2164, 10.5194/acp-13-2153-2013, 2013.

Riva, M., Heikkinen, L., Bell, D. M., Peräkylä, O., Zha, Q., Schallhart, S., Rissanen, M. P., Imre, D., Petäjä, T., Thornton, J. A., Zelenyuk, A. and Ehn, M.: Chemical transformations in monoterpene-derived organic aerosol enhanced by inorganic composition, npj Climate and Atmospheric Science, 2, 10.1038/s41612-018-0058-0, 2019.

Roberts, G. C. and Nenes, A.: A Continuous-Flow Streamwise Thermal-Gradient CCN Chamber for Atmospheric Measurements, Aerosol Sci. Technol., 39, 206-221, 10.1080/027868290913988, 2005.

https://doi.org/10.5194/egusphere-2025-39
Preprint. Discussion started: 7 January 2025
© Author(s) 2025. CC BY 4.0 License.

Roldin, P., Ehn, M., Kurtén, T., Olenius, T., Rissanen, M. P., Sarnela, N., Elm, J., Rantala, P., Hao, L., Hyttinen, N., Heikkinen, L., Worsnop, D. R., Pichelstorfer, L., Xavier, C., Clusius, P., Öström, E., Petäjä, T., Kulmala, M., Vehkamäki, H., Virtanen, A., Riipinen, I. and Boy, M.: The role of highly oxygenated organic molecules in the Boreal aerosol-cloud-climate system, Nat. Commun., 10, https://doi.org/10.1038/s41467-019-12338-8, 2019.

Saunders, S. M., Jenkin, M. E., Derwent, R. G. and Pilling, M. J.: Protocol for the development of the Master Chemical Mechanism, MCM v3 (Part A): tropospheric degradation of non-aromatic volatile organic compounds, Atmos. Chem. Phys., 3, 161–180, https://doi.org/10.5194/acp-3-161-2003, 2003.

Seibert, P. and Frank, A.: Source-receptor matrix calculation with a Lagrangian particle dispersion model in backward mode, Atmos. Chem. Phys., 4, 51-63, 10.5194/acp-4-51-2004, 2004.

Sindelarova, K., Markova, J., Simpson, D., Huszar, P., Karlicky, J., Darras, S. and Granier, C.: High-resolution biogenic global emission inventory for the time period 2000–2019 for air quality modelling, Earth Syst. Sci. Data, 14, 251-270, 10.5194/essd-14-251-2022, 2022.

Sipilä, M., Berndt, T., Petäjä, T., Brus, D., Vanhanen, J., Stratmann, F., Patokoski, J., Mauldin, R. L., Hyvärinen, A.-P., Lihavainen, H. and Kulmala, M.: The Role of Sulfuric Acid in Atmospheric Nucleation, Science, 327, 1243-1246, 10.1126/science.1180315, 2010.

Soulie, A., Granier, C., Darras, S., Zilbermann, N., Doumbia, T., Guevara, M., Jalkanen, J.-P., Keita, S., Liousse, C., Crippa, M., Guizzardi, D., Hoesly, R. and Smith, S.: Global Anthropogenic Emissions (CAMS-GLOB-ANT) for the Copernicus Atmosphere Monitoring Service Simulations of Air Quality Forecasts and Reanalyses, 10.5194/essd-2023-306, 2023.

Stohl, A., Forster, C., Frank, A., Seibert, P. and Wotawa, G.: Technical note: The Lagrangian particle dispersion model FLEXPART version 6.2, Atmos. Chem. Phys., 5, 2461–2474, https://doi.org/10.5194/acp-5-2461-2005, 2005.

Stohl, A., Hittenberger, M. and Wotawa, G.: Validation of the lagrangian particle dispersion model FLEXPART against large-scale tracer experiment data, Atmos. Environ., 32, 4245-4264, 10.1016/s1352-2310(98)00184-8, 1998.

Stohl, A. and Thomson, D. J.: A density correction for Lagrangian particle dispersion models, Bound.-Layer Met., 90, 155-167, 1999.

Stolzenburg, D., Fischer, L., Vogel, A. L., Heinritzi, M., Schervish, M., Simon, M., Wagner, A. C., Dada, L., Ahonen, L. R., Amorim, A., Baccarini, A., Bauer, P. S., Baumgartner, B., Bergen, A., Bianchi, F., Breitenlechner, M., Brilke, S., Buenrostro Mazon, S., Chen, D., Dias, A., Draper, D. C., Duplissy, J., El Haddad, I., Finkenzeller, H., Frege, C., Fuchs, C., Garmash, O., Gordon, H., He, X., Helm, J., Hofbauer, V., Hoyle, C. R., Kim, C., Kirkby, J., Kontkanen, J., Kürten, A., Lampilahti, J., Lawler, M., Lehtipalo, K., Leiminger, M., Mai, H., Mathot, S., Mentler, B., Molteni, U., Nie, W., Nieminen, T., Nowak, J. B., Ojdanic, A., Onnela, A., Passananti, M., Petäjä, T., Quéléver, L. L. J., Rissanen, M. P., Sarnela, N., Schallhart, S., Tauber, C., Tomé, A., Wagner, R., Wang, M., Weitz, L., Wimmer, D., Xiao, M., Yan, C., Ye, P., Zha, Q., Baltensperger, U., Curtius, J., Dommen, J., Flagan, R. C., Kulmala, M., Smith, J. N., Worsnop, D. R., Hansel, A., Donahue, N. M. and Winkler, P. M.: Rapid growth of organic aerosol nanoparticles over a wide tropospheric temperature range, Proc. Natl. Acad. Sci., 115, 9122-9127, 10.1073/pnas.1807604115, 2018.

Stolzenburg, D., Wang, M., Schervish, M. and Donahue, N. M.: Tutorial: Dynamic organic growth modeling with a volatility basis set, J. Aerosol Sci., 166, 106063, 10.1016/j.jaerosci.2022.106063, 2022.

https://doi.org/10.5194/egusphere-2025-39
Preprint. Discussion started: 7 January 2025
© Author(s) 2025. CC BY 4.0 License.

Svensmark, H., Enghoff, M. B., Svensmark, J., Thaler, I. and Shaviv, N. J.: Supersaturation and Critical Size of Cloud Condensation Nuclei in Marine Stratus Clouds, Geophys. Res. Lett., 51, 10.1029/2024gl108140, 2024.

Taipale, R., Ruuskanen, T. M., Rinne, J., Kajos, M. K., Hakola, H., Pohja, T. and Kulmala, M.: Technical Note: Quantitative long-term measurements of VOC concentrations by PTR-MS – measurement, calibration, and volume mixing ratio calculation methods, Atmos. Chem. Phys., 8, 6681-6698, 10.5194/acp-8-6681-2008, 2008.

Tørseth, K., Aas, W., Breivik, K., Fjæraa, A. M., Fiebig, M., Hjellbrekke, A. G., Lund Myhre, C., Solberg, S. and Yttri, K. E.: Introduction to the European Monitoring and Evaluation Programme (EMEP) and observed atmospheric composition change during 1972–2009, Atmos. Chem. Phys., 12, 5447-5481, 10.5194/acp-12-5447-2012, 2012.

Vana, M., Komsaare, K., Hõrrak, U., Mirme, S., Nieminen, T., Kontkanen, J., Manninen, H., Petäjä, T., Noe, S. and Kulmala, M.: Characteristics of new-particle formation at three SMEAR stations, Boreal Environ. Res., 21, 345-362, 2016.

Vouitsis, I., Ntziachristos, L. and Han, Z.: Methodology for the quantification of road transport PM emissions, using emission factors or profiles, TRANSPHORM Deliverable D, 1, 1-2, 2013.

Wang, Z., Ehn, M., Rissanen, M. P., Garmash, O., Quéléver, L., Xing, L., Monge-Palacios, M., Rantala, P., Donahue, N. M., Berndt, T. and Sarathy, S. M.: Efficient alkane oxidation under combustion engine and atmospheric conditions, Communications Chemistry, 4, 10.1038/s42004-020-00445-3, 2021.

Williams, J., Crowley, J., Fischer, H., Harder, H., Martinez, M., Petäjä, T., Rinne, J., Bäck, J., Boy, M., Dal Maso, M., Hakala, J., Kajos, M., Keronen, P., Rantala, P., Aalto, J., Aaltonen, H., Paatero, J., Vesala, T., Hakola, H., Levula, J., Pohja, T., Herrmann, F., Auld, J., Mesarchaki, E., Song, W., Yassaa, N., Nölscher, A., Johnson, A. M., Custer, T., Sinha, V., Thieser, J., Pouvesle, N., Taraborrelli, D., Tang, M. J., Bozem, H., Hosaynali-Beygi, Z., Axinte, R., Oswald, R., Novelli, A., Kubistin, D., Hens, K., Javed, U., Trawny, K., Breitenberger, C., Hidalgo, P. J., Ebben, C. J., Geiger, F. M., Corrigan, A. L., Russell, L. M., Ouwersloot, H. G., Vilà-Guerau de Arellano, J., Ganzeveld, L., Vogel, A., Beck, M., Bayerle, A., Kampf, C. J., Bertelmann, M., Köllner, F., Hoffmann, T., Valverde, J., González, D., Riekkola, M.-L., Kulmala, M. and Lelieveld, J.: The summertime Boreal forest field measurement intensive (HUMPPA-COPEC-2010): an overview of meteorological and chemical influences, Atmos. Chem. Phys., 11, 10599-10618, 10.5194/acp-11-10599-2011, 2011.

Xavier, C., Baykara, M., de Jonge, R. W., Altstädter, B., Clusius, P., Vakkari, V., Thakur, R., Beck, L., Becagli, S., Severi, M., Traversi, R., Wehner, B., Sipilä, M., Kulmala, M., Boy, M. and Roldin, P.: Secondary aerosol formation in marine Arctic environments: A model measurement comparison at Ny-Ålesund, Atmos. Chem. Phys., 22, 10023–10043, https://doi.org/10.5194/acp-22-10023-2022, 2022.

Yli-Juuti, T., Mielonen, T., Heikkinen, L., Arola, A., Ehn, M., Isokääntä, S., Keskinen, H.-M., Kulmala, M., Laakso, A., Lipponen, A., Luoma, K., Mikkonen, S., Nieminen, T., Paasonen, P., Petäjä, T., Romakkaniemi, S., Tonttila, J., Kokkola, H. and Virtanen, A.: Significance of the organic aerosol driven climate feedback in the boreal area, Nat. Commun., 12, 10.1038/s41467-021-25850-7, 2021.

Yu, F. and Luo, G.: Simulation of particle size distribution with a global aerosol model: contribution of nucleation to aerosol and CCN number concentrations, Atmos. Chem. Phys., 9, 7691-7710, 10.5194/acp-9-7691-2009, 2009.

Yu, S., Eder, B., Dennis, R., Chu, S. and Schwartz, S. E.: New unbiased symmetric metrics for evaluation of air quality models, Atmos. Sci. Lett., 7, 26-34, 10.1002/asl.125, 2006.

https://doi.org/10.5194/egusphere-2025-39
Preprint. Discussion started: 7 January 2025
© Author(s) 2025. CC BY 4.0 License.

Zhang, Y., Sheesley, R. J., Schauer, J. J., Lewandowski, M., Jaoui, M., Offenberg, J. H., Kleindienst, T. E. and Edney, E. O.: Source apportionment of primary and secondary organic aerosols using positive matrix factorization (PMF) of molecular markers, Atmos. Environ., 43, 5567-5574, 10.1016/j.atmosenv.2009.02.047, 2009.

Zhao, B., Donahue, N. M., Zhang, K., Mao, L., Shrivastava, M., Ma, P.-L., Shen, J., Wang, S., Sun, J., Gordon, H., Tang, S., Fast, J., Wang, M., Gao, Y., Yan, C., Singh, B., Li, Z., Huang, L., Lou, S., Lin, G., Wang, H., Jiang, J., Ding, A., Nie, W., Qi, X., Chi, X. and Wang, L.: Global variability in atmospheric new particle formation mechanisms, Nature, 631, 98-105, 10.1038/s41586-024-07547-1, 2024.

Zhou, P., Ganzeveld, L., Rannik, Ü., Zhou, L., Gierens, R., Taipale, D., Mammarella, I. and Boy, M.: Simulating ozone dry deposition at a boreal forest with a multi-layer canopy deposition model, Atmos. Chem. Phys., 17, 1361-1379, 10.5194/acp-17-1361-2017, 2017.